Smart Structures and Systems, *Vol. 23, No. 5 (2019) 429-447*
DOI: https://doi.org/10.12989/sss.2019.23.5.429

Size-dependent magneto-electro-elastic vibration analysis of FG saturated porous annular/ circular micro sandwich plates embedded with nano-composite face sheets subjected to multi-physical pre loads

Saeed Amir*[1], Ehsan Arshid[1] and Mohammad Reza Ghorbanpour Arani[2]

[1]*Department of Solid Mechanics, Faculty of Mechanical Engineering, University of Kashan, Kashan, Iran*
[2]*Electrical Engineering Department, Amirkabir University of Technology, Tehran, Iran*

(Received December 24, 2018, Revised March 10, 2019, Accepted March 14, 2019)

Abstract. The present study analyzed free vibration of the three-layered micro annular/circular plate which its core and face sheets are made of saturated porous materials and FG-CNTRCs, respectively. The structure is subjected to magneto-electric fields and magneto-electro-mechanical pre loads. Mechanical properties of the porous core and also FG-CNTRC face sheets are varied through the thickness direction. Using dynamic Hamilton's principle, the motion equations based on MCS and FSD theories are derived and solved via GDQ as an efficient numerical method. Effect of different parameters such as pores distributions, porosity coefficient, pores compressibility, CNTs distribution, elastic foundation, multi-physical pre loads, small scale parameter and aspect ratio of the plate are investigated. The findings of this study can be useful for designing smart structures such as sensor and actuator.

Keywords: free vibration; modified couple stress theory; porous material; carbon nanotubes reinforced composites; circular sandwich plate; pasternak foundation

1. Introduction

By advancement the material science, the researchers are encouraged to study more about new materials and consider their effects on the engineering structures mechanical behaviors such as bending, buckling, and vibrations. Nowadays porous materials are one of the most important materials in the engineering structures and by considering their effect, theoretical results will be near to the experimental ones. Biot (1964) is the pioneer to study about poroelasticity. In his model, the porous materials are consist of two parts: the solid and fluid phases. The constitutive relations for saturated porous materials regarding the mentioned phases presented by Detournay and Cheng (1995). Theodorakopoulos and Beskos (1994) studied about flexural vibrations of poroelastic plates. They used Kirchhoff assumptions to derive the governing equations for the rectangular plate which was subjected to harmonic load using the analytical-numerical method and used Biot's model for the porous material. Leclaire *et al.* (2001) investigated the vibration of a porous rectangular plate which was filled by a fluid. They used classical plates theory (CPT) and assumed that the porosity distributed uniformly across the thickness. They considered the effect of porosity and other important parameters on the results. Chen *et al*. (2016) presented their research about porous beams and sandwich beams with a porous core with accounting the large amplitude deformations. They considered different distribution types of pores in their studies and investigated the effect of porous materials properties on the results. Khorshidvand *et al.* (2014) studied about buckling of a circular plate which was integrated by piezoelectric sensor- actuator layers. They considered the effect of the piezoelectric patches, feedback gain and shape parameters of the clamped plate on the results. Arshid and Khorshidvand (2017) studied about a porous solid circular plate based on CPT. They presented another study about its vibration by integrating the mentioned structure with piezoelectric actuators and considered the effect of structure and piezoelectric actuators on the natural frequencies (Arshid and Khorshidvand 2018). They found out generally the porosity increasing, causes decreasing in natural frequency. Ebrahimi *et al*. (2017a) studied about the vibration of magneto-electro elastic (MEE) porous rectangular plates using tangential shear deformation plates theory. They account neutral axis position and used power-law model for describing the pores distribution. Also, a study about mechanical behavior of FGMEE skew plates carried out by Kiran and Kattimani (2018). They used the finite element method (FEM) to obtain the results for free vibration and static responses. The motion equations of a porous rectangular plate were solved analytically by Rezaei and Saidi (2015). They considered the effect of the fluid in pores and assumed that the pores distribution obey cosine function through the thickness and employed Reddy's TSDT to obtain the equations and solved them for a specific boundary condition analytically. Barati *et al.* (2017) investigated the vibration of piezoelectric FG plates with porosities. Their study was based on a refined four-variable theory and used the power-law model for pores distribution.

*Corresponding author, Assistant Professor
E-mail: samir@kashanu.ac.ir

ISSN: 1738-1584 (Print), 1738-1991 (Online)

They discussed about applied voltage, porosity, and other parameters effects on the results.

Also, reinforced composites are recently used to refine the properties of the structures. One of the best and well-known reinforcements of the composites are carbon nanotubes (CNTs). Iijima has been discovered CNTs in the 1990s (Iijima 1991) and after that by doing researches by the others, it was found that because of very high elastic modulus and magnetic feature, they can be so useful and valuable. Consequently, carbon nanotubes reinforced composites (CNTRCs) are used as an important part of engineering structures which the desired properties are needed. It is noteworthy that CNTs are usually used as reinforcement for the polymeric composites and their arrangement direction is one of the most important factors to obtain the mechanical properties of CNTRCs. Depends on the matrix properties, the CNTRCs have a wide range of usage. For example, by using Polyvinylidene fluoride (PVDF) which has the magnetic properties as the matrix, they can be used in magneto and electro engineering, aerospace industries, MEMS and NEMS (Abdel-Rahman *et al*. 2002, Ashrafi *et al.* 2006).

In recent years study about the beams, shells and plates are developing and the researchers are trying to use new methods to improve their behaviors. Using sandwich structure is one of the best ways to achieve this goal. A soft core in comparison to stiffer face sheets is one of the most important features of the sandwich structures. So choosing appropriate material as core and face sheets are important to achieve the best desired results. Ferreira *et al.* (2013) used generalized differential quadrature method (GDQM) to obtain the frequencies of a sandwich plate. An efficient meshfree method for vibration analysis of laminated composite plates presented by Bui *et al.* (2011). Static and dynamic stability of FG plates and shells in nonlinear form investigated by Duc (2014). A CNTRC plate vibration analysis was performed via FEM based on the first order shear deformation theory (FSDT) by Zhu *et al.* (2012). Their analysis was for different kinds of CNTs distributions and obtained the bending response, natural frequencies for various boundary conditions. Nonlinear stability analysis of imperfect three-phase sandwich laminated polymer nanocomposite panels in thermal environments presented by Pham and Duc (2016). Loghman and Cheraghbak (2018) considered agglomeration effects on the behavior of nano-composite piezoelectric cylinder. They assumed that the structure was under an internal pressure and CNTs selected as the reinforcement of the composite. Mirzaei and Kiani (2016) used the refined rule mixture to analyze FG-CNTRC cylindrical panels. They considered CNTs different effects on the results. Lei *et al.* (2013) applied the Ritz method to analyze vibration of FG-CNTRC plates. The plate was in a thermal environment and they considered both uniform and FG distribution of CNTs and studied about the effect of different parameters on the results. Nonlinear thermo-electro-mechanical dynamic response of shear deformable piezoelectric Sigmoid FG sandwich circular cylindrical shells presented by Duc (2018). Also, Mehar *et al*. (2017) used FEM to solve the nonlinear equations of a doubly curved FG-CNTRC shell. The structure was in a thermal environment and was modeled based on higher-order kinematics theory and Green-Lagrange geometrical nonlinear strains. Nonlinear thermo-mechanical buckling and post-buckling response of porous FGM plates using Reddy's theory carried out by Cong *et al.* (2018). In another study, Duc *et al.* (2018) investigated nonlinear dynamic response of FGM porous plates on elastic foundation subjected to thermal and mechanical loads using the FSDT. CNTRCs are also used as face sheets in sandwich structures. FSDT used by Amir *et al.* (2018a) to study about buckling behavior of the nano-composite sandwich plate regarding the flexoelectricity effects. They used the analytical method to obtain the results. The vibration of a magnetorheological (MR) fluid plate which was placed between two nano-composite layers studied by Ghorbanpour Arani *et al.* (2018). The face sheets of the considered plate were piezoelectric nano-composite. They concluded increasing the CNTs caused the higher stiffness for the structure. Wang and Shen (2012) presented a nonlinear analysis of sandwich plates with CNTRC face sheets. They assumed that the properties of the face sheets were varied by temperature changes and considered the effect of temperature variations on the results. Effect of high temperature on mechanical behaviors of heated FG plates was considered by Bui *et al.* (2016) based on a new third-order shear deformation theory. They found not all FGMs possess similar mechanical behaviors and performance in high temperature. Also, Do *et al.* (2017) investigated material combinations effect on the mechanical behavior of FG sandwich plates in thermal environment. Nonlinear dynamic and vibration of sigmoid power law distribution FGM elliptical cylindrical shells surrounded on elastic foundations in thermal environments analyzed by Duc *et al.* (2017). Moreover, Duc (2016) employed Reddy's third-order shear deformation shell theory to analyzed nonlinear thermal dynamic of eccentrically stiffened circular cylindrical shells. Effect of temperature-dependent properties on the dynamic behavior of imperfect FGM double curved thin shallow shells discussed by Duc and Quan (2015). Mechanical behavior of shear deformable eccentrically stiffened sigmoid power law distribution FGM cylindrical panels resting on elastic foundation carried out by Quan *et al*. (2015). The formulation of an annular sector plate with piezoelectric layers have been derived regarding large amplitude deformation, using FSDT and Von-Karman assumption for strain-displacement relations presented by Mohammadzadeh-Keleshteri *et al.* (2017) and GDQM has been employed to solve the equations.

Due to the difference in results of the macro and small scales analysis, the researchers have been interested to study about small scale behavior of the structures. Eringen is from the first researchers who has been studied about the structures in the small dimensions and especially nano one which his theory called nonlocal (Eringen 1983, 2002). After Eringen's studies, the study about small scales effects extended rapidly and other researches also find out new hints (Ghorbanpour Arani *et al.* 2013a, b, 2016, Mechab *et al.* 2016). Also, Ghorbanpour Arani and Zamani (2018) considered porosity and size effects on the vibration of a porous sandwich plate. Amir *et al.* (2018b) analyzed the

vibration of a rectangular porous nano sandwich plate based on sinusoidal shear deformation (SSDT) and nonlocal theories. They solved the equations using Navier's solution method and discussed influence of different parameters on the results in details. Through time and doing various researches using nonlocal theory and finding out its defects, other small scales theories were presented (Shafiei and Kazemi 2017, Shafiei *et al*. 2017, Shahverdi and Barati 2017). Modified couple stress (MCS) and modified strain gradient theories are the featured of them which are often used for micro scales. Loghman *et al.* (2017) researched about the stability of non-axisymmetric FG-CNTRC micro plates. They used MCST to account the size effects. Liu *et al.* (2017a) analyzed vibration, buckling and bending behaviors of homogenous and FG micro plates using MCST, based on non-classical Kirchhoff's theory and discussed small scale effect on the results. In another study, Liu *et al.* (2017b) considered mechanical behaviors of a moderately thick micro plate based on FSD and MCS theories. Liu *et al.* (2018) also presented an effective numerical model based on extended isogeometric analysis for assessment of vibration and buckling of FG microplates with cracks. They captured the size effects using MCST. Kolahdouzan *et al*. (2018) analyzed FG-CNTRC micro sandwich plate based on MCST. Their work focused on the buckling and vibration response of the plate. A novel MCST based size-dependent quasi-3D isogeometric beam model for two-directional FG microbeams presented by Yu *et al.* (2019b). The influences of material gradient factors along the axial and thickness directions, material length scale factor, boundary condition, and other aspect ratios of two-directional FG microbeams on mechanical behavior were investigated in their study. A computational approach for mechanical behavior of nanoplates presented Liu *et al.* (2019). The MCST was used to capture the microstructural effect and they concluded that both microstructure and surface energy effects increase the rigidity of nanoplates. Size-dependent behaviors of thick FG microbeams investigated by Yu *et al.* (2019a). To capture the size effects, they employed an extension of quasi-3D theory to integrate with the MCST.

The current study aims to analyze vibration of the annular/ circular micro sandwich plate which its core is made of saturated porous material which is presented based on Biot's model and the face sheets are made of FG-CNTRCs. The properties of the porous core are varying through its thickness according to the given functions which are related to pores placement and the mechanical properties of the FG-CNTRCs face sheets based on CNTs distribution, follows five different types. Using MCST and based on the FSDT which is more complex rather than CPT and account shear deformations effect, the motion equations are obtained. Using GDQM which is known as an accurate and rapid-converge numerical method, the equations will be solved for various boundary conditions. The results will be verified for the simpler states in the literature and effect of different materials parameters and geometric size of the plate will be presented and will be discussed about them in details. Reviewing the literature showed there is no study about such a plate and the novelty of the present work is considering three-layered annular/circular saturated porous micro plate which is integrated by FG-CNTRC face sheets and is subjected to magneto-electric fields and multi-physical pre loads. The findings of this work will help to design and create more optimal engineering and smart structures such as sensors and actuators.

2. Theoretical relations

As shown in Fig. 1 three-layered micro annular and circular plates with the porous core and FG-CNTRC face sheets are under consideration. The inner and outer radius of the plate are shown by b and a, respectively and h_c, h_t and h_b represent the thickness of the core, top, and bottom layers. The structure is resting on Pasternak type of elastic foundation and is under magneto electro-mechanical pre loads. The origin of the cylindrical coordinate system (r,θ,z) which is used to describe the displacements is at the center of the middle plane.

2.1 MCST

According to MCST the strain energy is as follow (Reddy and Berry 2012)

$$U_M = \frac{1}{2}\int_r\int_\theta\int_z \left(\sigma : \varepsilon + \mathrm{m} : \chi\right) r \,\mathrm{d}r\,\mathrm{d}\theta\,\mathrm{d}z \tag{1}$$

where σ, ε, m and χ are the symmetric part of the Cauchy stress, strain, deviator part of the couple stress and the symmetric curvature tensors, respectively and the subscript M refers to MCST. The mentioned tensors are defined as follows (Ke *et al*. 2012)

$$\sigma = \lambda\,\mathrm{tr}(\varepsilon)\mathrm{I} + 2\mu\varepsilon, \tag{2}$$

$$\varepsilon = \frac{1}{2}\left[\nabla \mathrm{u} + (\nabla \mathrm{u})^T\right], \tag{3}$$

$$\mathrm{m} = 2l_m^2\mu\chi, \tag{4}$$

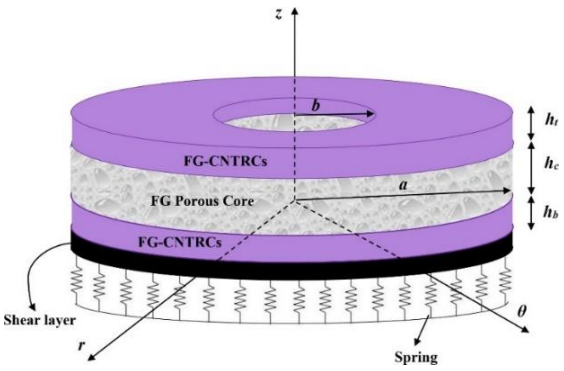

Fig. 1 Schematic of the considering sandwich annular/ circular micro plate with saturated porous core and FG-CNTRCs face sheets resting on Pasternak foundation

$$\chi = \frac{1}{2}\left[\nabla\Theta + \left(\nabla\Theta\right)^{T}\right] \tag{5}$$

where u represents the displacement vector, Lame's constant are shown by λ and μ, l_m is the parameter of the material length scale, and rotation vector is presented by Θ which is defined as

$$\Theta = \frac{1}{2}\nabla \times \mathrm{u} \tag{6}$$

2.2 Displacement components and strains

According to the FSDT which accounts the shear deformation effects, the displacements are as (Reddy and Khdeir 1989, Arshid *et al.* 2019)

$$\begin{aligned} u(r,\theta,z,t) &= u_0(r,\theta,t) + z\lambda_r(r,\theta,t), \\ v(r,\theta,z,t) &= v_0(r,\theta,t) + z\lambda_\theta(r,\theta,t), \\ w(r,\theta,z,t) &= w_0(r,\theta,t) \end{aligned} \tag{7}$$

where u, v and w are the displacements of an arbitrary point of the structure in r, θ and z directions, respectively and u_0, v_0 and w_0 represent the displacements of the middle plane of the plate in the mentioned directions. Also, λ_r and λ_θ are the transverse normal rotation about the θ and r axes, respectively.

The strain-displacement relations in the cylindrical coordinate system are given as (Brush *et al*. 1975)

$$\begin{aligned} \varepsilon_{rr} &= \frac{\partial u}{\partial r}, \qquad \varepsilon_{\theta\theta} = \frac{1}{r}\frac{\partial v}{\partial \theta} + \frac{u}{r}, \\ \gamma_{rz} &= \frac{\partial u}{\partial z} + \frac{\partial w}{\partial r}, \qquad \gamma_{\theta z} = \frac{\partial v}{\partial z} + \frac{1}{r}\frac{\partial w}{\partial \theta} \\ \gamma_{r\theta} &= \frac{1}{r}\frac{\partial u}{\partial \theta} - \frac{v}{r} + \frac{\partial v}{\partial r}, \end{aligned} \tag{8}$$

Substituting displacement components from Eq. (7) to strain-displacement relations, yields

$$\begin{aligned} \varepsilon_{rr} &= \frac{\partial u_0}{\partial r} + z\frac{\partial \lambda_r}{\partial r}, \\ \varepsilon_{\theta\theta} &= \frac{1}{r}\frac{\partial v_0}{\partial \theta} + \frac{u_0}{r} + z\left(\frac{1}{r}\frac{\partial \lambda_\theta}{\partial \theta} + \frac{1}{r}\lambda_r\right), \\ \gamma_{r\theta} &= \frac{1}{r}\frac{\partial u_0}{\partial \theta} - \frac{v_0}{r} + \frac{\partial v_0}{\partial r} + z\left(\frac{1}{r}\frac{\partial \lambda_r}{\partial \theta} - \frac{1}{r}\lambda_\theta + \frac{\partial \lambda_\theta}{\partial r}\right), \\ \gamma_{rz} &= \lambda_r + \frac{\partial w_0}{\partial r}, \\ \gamma_{\theta z} &= \lambda_\theta + \frac{1}{r}\frac{\partial w_0}{\partial \theta} \end{aligned} \tag{9}$$

2.3 Material properties

2.3.1 Porous core

In order to determine the structure's properties, firstly the porous core will be considered. The stress-strain relation for the saturated porous core is as follow (Detournay and Cheng 1995)

$$\sigma_{ij}^{c} = 2G(z)\varepsilon_{ij} + \lambda\varepsilon\delta_{ij} - \alpha(z)P_p\delta_{ij} \tag{10}$$

in which

$$\lambda = \frac{2G(z)\nu_u}{1-2\nu_u}, \tag{11}$$

$$P_p = M\left(\zeta - \alpha\varepsilon\right), \tag{12}$$

$$M = \frac{2G(z)(\nu_u - \nu)}{\alpha^2(1-2\nu_u)(1-2\nu)}, \tag{13}$$

$$\nu_u = \frac{\nu + \alpha B(1-2\nu)/3}{1-\alpha B(1-2\nu)/3} \tag{14}$$

In the above relations, $G(z)$ is the shear modulus, ε is the volumetric strain which is defined as $\varepsilon_{rr}+\varepsilon_{\theta\theta}+\varepsilon_{kk}$, δ_{ij} is the Kronecker delta, $\alpha(z)$ is the Biot coefficient and is equal to $1\text{-}G(z)/G_0$. Also, P_p is the pore fluid pressure, M is the Biot modulus and ζ is the variations of the fluid in the pores and for the undrained condition, ζ is equal to zero. In this condition, the pores pressure can be simplified as follow

$$P_p = M\left(-\alpha\varepsilon\right) \tag{15}$$

Poisson's ratio in drained and undrained conditions are defined as the following

$$\nu = -\frac{\varepsilon_{jj}}{\varepsilon_{ii}}\Big|_{\sigma_{jj}=0}, \qquad P_p = 0 \tag{16}$$

$$\nu_u = -\frac{\varepsilon_{jj}}{\varepsilon_{ii}}\Big|_{\sigma_{jj}=0}, \qquad \zeta = 0 \tag{17}$$

Also, B is the Skempton coefficient which expresses the pressure of the fluids within the pores.

Consequently, the stress-strain relation for the undrained condition of the porous core can be rewritten as follow

$$\sigma_{ij}^{c} = 2G(z)\varepsilon_{ij} + \left(\lambda + M\alpha^2\right)\varepsilon\delta_{ij} \tag{18}$$

Using the plane stress assumption, the stress components of the porous core in terms of strains can are as the following

$$\begin{Bmatrix} \sigma_{rr} \\ \sigma_{\theta\theta} \\ \sigma_{rz} \\ \sigma_{\theta z} \\ \sigma_{r\theta} \end{Bmatrix} = \begin{bmatrix} A_1(z) & B_1(z) & 0 & 0 & 0 \\ B_1(z) & A_1(z) & 0 & 0 & 0 \\ 0 & 0 & \kappa_f G(z) & 0 & 0 \\ 0 & 0 & 0 & \kappa_f G(z) & 0 \\ 0 & 0 & 0 & 0 & G(z) \end{bmatrix} \begin{Bmatrix} \varepsilon_{rr} \\ \varepsilon_{\theta\theta} \\ \gamma_{rz} \\ \gamma_{\theta z} \\ \gamma_{r\theta} \end{Bmatrix} \tag{19}$$

in which κ_f is the shear correction factor of FSDT and for circular plate is equal to $\pi^2/12$ and

$$A_1(z)=2\frac{1-4\nu+2\nu_u}{1-3\nu+2\nu\nu_u}G(z), \tag{20}$$

$$B_1(z)=2\frac{-\nu+2(1-\nu)\nu_u}{1-3\nu+2\nu\nu_u}G(z) \tag{21}$$

The attributes of the porous core are varied across its thickness. So, three functions called porosity distribution are considered. The general relations for Young's elasticity modulus and density of these three types are as follow

$$\begin{aligned} E(z)&=E_0\ f(z),\\ \rho(z)&=\rho_0\ g(z) \end{aligned} \tag{22}$$

For the nonlinear non-symmetric porosity distribution, E and ρ depend on z as (Arshid and Khorshidvand 2018)

$$\begin{aligned} f(z)&=1-e_1\cos\left[\frac{\pi}{2h_c}\left(z+\frac{h_c}{2}\right)\right]\\ g(z)&=1-e_m\cos\left[\frac{\pi}{2h_c}\left(z+\frac{h_c}{2}\right)\right] \end{aligned} \tag{23}$$

where h_c is the thickness of the porous core and the porosity coefficient is shown by e_1 which indicates the pores to total volume ratio ($0 < e_1 < 1$). Also, this coefficient can be defined as follow

$$e_1=1-\frac{E_1}{E_0}, \tag{24}$$

in which E_1 and E_0 are the minimum and maximum values of Young's elasticity modulus which occur at the bottom and top surfaces of the core, respectively.

e_m is called mas density coefficient and is introduced in terms of densities and porosity coefficient as (Amir *et al.* 2018b)

$$e_m=1-\frac{\rho_1}{\rho_0}=1-\sqrt{1-e_1}, \tag{25}$$

Similar to moduli of elasticity, ρ_1 and ρ_0 are densities of the core.

For the nonlinear symmetric porosity distribution, E and ρ are distributed based on a symmetric cosine function as (Arshid and Khorshidvand 2018)

$$\begin{aligned} f(z)&=1-e_1\cos\left(\frac{\pi z}{h_c}\right),\\ g(z)&=1-e_m\cos\left(\frac{\pi z}{h_c}\right) \end{aligned} \tag{26}$$

And for the monotonous porosity distribution, E and ρ are independent of z and are given as (Arshid and Khorshidvand 2018)

$$\begin{aligned} f(z)&=1-e_1\chi,\\ g(z)&=\sqrt{1-e_1\chi} \end{aligned} \tag{27}$$

where

$$\chi=\frac{1}{e_1}-\frac{1}{e_1}\left(\frac{2}{\pi}\sqrt{1-e_1}-\frac{2}{\pi}+1\right)^2 \tag{28}$$

2.3.2 FG-CNTRCs Face sheets

Extended mixture rule is employing to determine the effective properties of face sheets. According to this rule the mechanical properties of the face sheets i.e., Young's and shear moduli can be achieved using the following relations (Arani *et al.* 2015)

$$E_{11}=\eta_1 V_{CNT}E_{11}^{CNT}+V_mE_m \tag{29}$$

$$\frac{\eta_2}{E_{22}}=\frac{V_{CNT}}{E_{22}^{CNT}}+\frac{V_m}{E_m} \tag{30}$$

$$\frac{\eta_3}{G_{12}}=\frac{V_{CNT}}{G_{12}^{CNT}}+\frac{V_m}{G_m} \tag{31}$$

in which E_{11}^{CNT}, E_{22}^{CNT}, G_{12}^{CNT}, E_m and G_m are longitudinal and transversely Young's and shear moduli of the CNTs and matrix, respectively. Also, V_{CNT} is volume fraction of CNTs which is determined for different types of CNTs distributions and V_m represents volume fraction of matrix and $V_{CNT}+V_m=1$. It should be noted that PVDF is considered as matrix in this paper. η_1, η_2, and η_3 are efficiency parameters of CNTs which are determined by molecular dynamics simulation.

Also, the mixture rule can be developed for other properties of the FG-CNTRCs face sheets i.e., magnetic and electric ones as follow (Loghman and Cheraghbak 2018)

$$P_{ij}=V_{CNT}P_{ij}^{CNT}+V_mP_{ij}^m \tag{32}$$

where P_{ij} represents the effective properties of the face sheets and P_{ij}^{CNT} and P_{ij}^m demonstrate the same property for the CNTs and matrix. P_{ij} indicates different mechanical and magneto-electric properties of the face sheets such as density, piezoelectric and magnetic coefficients, electro-magnetic coupling and dielectric and magnetic permeability. However, the Poisson's ratio varies through the following relation

$$\nu_{12}=V_{CNT}^*\nu_{12}^{CNT}+V_m\nu_m \tag{33}$$

It's clear that the Poisson's ratio does not depend on CNTs distribution. V_{CNT}^* is the volume fraction of CNTs and defined as follow

$$V_{CNT}^*=\frac{w_{CNT}}{w_{CNT}+\left(\frac{\rho_{CNT}}{\rho_m}\right)-\left(\frac{\rho_{CNT}}{\rho_m}\right)w_{CNT}} \tag{34}$$

in which w_{CNT} denotes the mass density of the CNTs and ρ_{CNT} and ρ_m are densities of the CNTs and matrix.

The CNTs are distributed symmetrically in the face sheets according to uniform and different FG types. Consequently, UU, FG-VA, FG-AV, FG-XX, FG-OO CNTs distribution types are considered in this study. It should be noted that the first letter is related to the top face sheet and the second one is for the bottom face sheet. The mentioned types are shown in Fig. 2 and their relation with CNTs volume fraction are as follow (Ghorbanpour Arani *et al*. 2018)

For the top face sheet

$$\begin{aligned}
&V_{CNT}^{t}=V_{CNT}^{*} && \text{UD}\\
&V_{CNT}^{t}=\left[1-\frac{2}{h_t}\left(z-\frac{h_c+h_t}{2}\right)\right]V_{CNT}^{*} && \text{FG-A}\\
&V_{CNT}^{t}=\left[1+\frac{2}{h_t}\left(z-\frac{h_c+h_t}{2}\right)\right]V_{CNT}^{*} && \text{FG-V}\\
&V_{CNT}^{t}=2\left[1-\frac{2}{h_t}\left(z-\frac{h_c+h_t}{2}\right)\right]V_{CNT}^{*} && \text{FG-O}\\
&V_{CNT}^{t}=\frac{4}{h_t}\left[\left|z-\frac{h_c+h_t}{2}\right|\right]V_{CNT}^{*} && \text{FG-X}
\end{aligned} \tag{35}$$

For the bottom face sheet

$$\begin{aligned}
&V_{CNT}^{b}=V_{CNT}^{*} && \text{UD}\\
&V_{CNT}^{b}=\left[1-\frac{2}{h_b}\left(z+\frac{h_c+h_b}{2}\right)\right]V_{CNT}^{*} && \text{FG-A}\\
&V_{CNT}^{b}=\left[1+\frac{2}{h_b}\left(z+\frac{h_c+h_b}{2}\right)\right]V_{CNT}^{*} && \text{FG-V}\\
&V_{CNT}^{b}=2\left[1-\frac{2}{h_b}\left(z+\frac{h_c+h_b}{2}\right)\right]V_{CNT}^{*} && \text{FG-O}\\
&V_{CNT}^{b}=\frac{4}{h_b}\left[\left|z+\frac{h_c+h_b}{2}\right|\right]V_{CNT}^{*} && \text{FG-X}
\end{aligned} \tag{36}$$

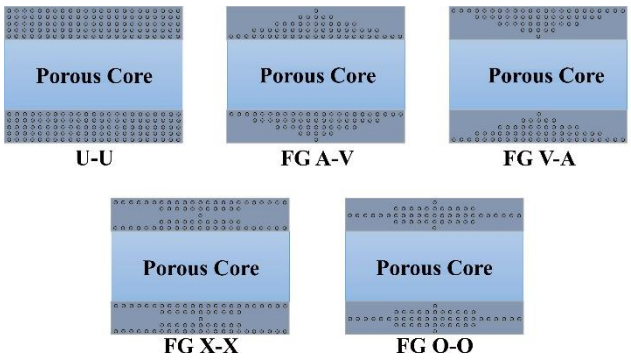

Fig. 2 Various distribution types of CNTs through the thickness of the face sheets

The stress-strain relations for FG-CNTRC face sheets in presence of magneto-electric fields may be written as

$$\begin{Bmatrix}\sigma_{rr}\\ \sigma_{\theta\theta}\\ \sigma_{rz}\\ \sigma_{\theta z}\\ \sigma_{r\theta}\end{Bmatrix}=\begin{bmatrix}Q_{11} & Q_{12} & 0 & 0 & 0\\ Q_{12} & Q_{22} & 0 & 0 & 0\\ 0 & 0 & \kappa_f Q_{55} & 0 & 0\\ 0 & 0 & 0 & \kappa_f Q_{44} & 0\\ 0 & 0 & 0 & 0 & Q_{66}\end{bmatrix}\begin{Bmatrix}\varepsilon_{rr}\\ \varepsilon_{\theta\theta}\\ \gamma_{rz}\\ \gamma_{\theta z}\\ \gamma_{r\theta}\end{Bmatrix}-\begin{bmatrix}0 & 0 & e_{31}\\ 0 & 0 & e_{32}\\ 0 & e_{24} & 0\\ e_{15} & 0 & 0\\ 0 & 0 & 0\end{bmatrix}\begin{Bmatrix}E_r\\ E_\theta\\ E_z\end{Bmatrix}-\begin{bmatrix}0 & 0 & q_{31}\\ 0 & 0 & q_{32}\\ 0 & q_{24} & 0\\ q_{15} & 0 & 0\\ 0 & 0 & 0\end{bmatrix}\begin{Bmatrix}H_r\\ H_\theta\\ H_z\end{Bmatrix} \tag{37}$$

Here, e_{ij} represent piezoelectric and q_{ij} magnetic coefficients, electric and magnetic fields are shown by E_i and H_i, respectively and Q_{ij} are stiffness matrix components and are defined as follow (Amir *et al*. 2018a)

$$\begin{aligned}
&Q_{11}=\frac{E_{11}}{1-\nu_{12}\nu_{21}}, && Q_{12}=\nu_{21}Q_{11}, && Q_{22}=\frac{E_{22}}{1-\nu_{12}\nu_{21}},\\
&Q_{44}=G_{23}, && Q_{55}=G_{13}, && Q_{66}=G_{12}.
\end{aligned} \tag{38}$$

Also, the electric and magnetic displacements can be introduced using the following relations (Ke and Wang 2014)

$$\begin{Bmatrix}D_r\\ D_\theta\\ D_z\end{Bmatrix}=\begin{bmatrix}0 & 0 & 0 & e_{15} & 0\\ 0 & 0 & e_{24} & 0 & 0\\ e_{31} & e_{32} & 0 & 0 & 0\end{bmatrix}\begin{Bmatrix}\varepsilon_{rr}\\ \varepsilon_{\theta\theta}\\ \gamma_{\theta z}\\ \gamma_{rz}\\ \gamma_{r\theta}\end{Bmatrix}+\begin{bmatrix}s_{11} & 0 & 0\\ 0 & s_{22} & 0\\ 0 & 0 & s_{33}\end{bmatrix}\begin{Bmatrix}E_r\\ E_\theta\\ E_z\end{Bmatrix}+\begin{bmatrix}d_{11} & 0 & 0\\ 0 & d_{22} & 0\\ 0 & 0 & d_{33}\end{bmatrix}\begin{Bmatrix}H_r\\ H_\theta\\ H_z\end{Bmatrix}, \tag{39}$$

$$\begin{Bmatrix}B_r\\ B_\theta\\ B_z\end{Bmatrix}=\begin{bmatrix}0 & 0 & 0 & q_{15} & 0\\ 0 & 0 & q_{24} & 0 & 0\\ q_{31} & q_{32} & 0 & 0 & 0\end{bmatrix}\begin{Bmatrix}\varepsilon_{rr}\\ \varepsilon_{\theta\theta}\\ \gamma_{\theta z}\\ \gamma_{rz}\\ \gamma_{r\theta}\end{Bmatrix}+\begin{bmatrix}d_{11} & 0 & 0\\ 0 & d_{22} & 0\\ 0 & 0 & d_{33}\end{bmatrix}\begin{Bmatrix}E_r\\ E_\theta\\ E_z\end{Bmatrix}+\begin{bmatrix}\mu_{11} & 0 & 0\\ 0 & \mu_{22} & 0\\ 0 & 0 & \mu_{33}\end{bmatrix}\begin{Bmatrix}H_r\\ H_\theta\\ H_z\end{Bmatrix}, \tag{40}$$

where s_{ii}, $d_{ii,}$ and μ_{ii} are dielectric permeability, magneto-electric coefficients and magnetic permeability, respectively and D_i and B_i represent electric and magnetic displacements.

To satisfy Maxwell's relations, the electric and magnetic fields can be defined as follow (Ghorbanpour Arani and Zamani 2017, Ellali *et al.* 2018)

$$E=-\nabla\Phi, \tag{41}$$

$$H=-\nabla\Psi \tag{42}$$

The electric and magnetic potentials are summation of cosine and linear terms as follows (Ke and Wang 2014)

$$\Phi(r,\theta,z,t)=\frac{2z}{h_f}\phi_0-\cos\left(\frac{\pi z}{h_f}\right)\phi(r,\theta,t), \tag{43}$$

$$\Psi(r,\theta,z,t)=\frac{2z}{h_f}\psi_0-\cos\left(\frac{\pi z}{h_f}\right)\psi(r,\theta,t) \tag{44}$$

where ϕ_0 and ψ_0 are the external applied electric and magnetic potentials, respectively and h_f is the thickness of each face sheet. According to Eqs. (41) and (42), the components of electric and magnetic fields are as

$$\begin{aligned}&\{E_r,E_\theta\}=-\left\{\frac{\partial\Phi}{\partial r},\frac{1}{r}\frac{\partial\Phi}{\partial\theta}\right\}=\left\{\frac{\partial\phi}{\partial r},\frac{1}{r}\frac{\partial\phi}{\partial\theta}\right\}\cos\left(\frac{\pi z}{h_f}\right),\\&E_z=-\frac{\partial\Phi}{\partial z}=-\frac{2}{h_f}\phi_0-\frac{\pi}{h_f}\phi\sin\left(\frac{\pi z}{h_f}\right)\end{aligned} \tag{45}$$

$$\begin{aligned}&\{H_r,H_\theta\}=-\left\{\frac{\partial\Psi}{\partial r},\frac{1}{r}\frac{\partial\Psi}{\partial\theta}\right\}=\left\{\frac{\partial\psi}{\partial r},\frac{1}{r}\frac{\partial\psi}{\partial\theta}\right\}\cos\left(\frac{\pi z}{h_f}\right),\\&H_z=-\frac{\partial\Psi}{\partial z}=-\frac{2}{h_f}\psi_0-\frac{\pi}{h_f}\psi\sin\left(\frac{\pi z}{h_f}\right)\end{aligned} \tag{46}$$

3. Motion equations and boundary conditions

3.1 Strain energy

The total strain energy of the three-layered annular/ circular is divided into two parts: the first part is for the modified couple stress as explained in Eqs. (1)-(6) and the second part is related to the classical structure.

$$U=U_c+U_M \tag{47}$$

in which U_c and U_M denote the strain energies of classical and MCST, respectively. Thus the strain energy of the plate can be achieved using the below relation (Ke *et al*. 2014)

$$\begin{aligned}U=&\frac{1}{2}\iint_{r\theta}\int_{-\frac{h_c}{2}-h_b}^{-\frac{h_c}{2}}\begin{Bmatrix}\sigma_{rr}^b\varepsilon_{rr}+\sigma_{\theta\theta}^b\varepsilon_{\theta\theta}+\sigma_{r\theta}^b\gamma_{r\theta}+\sigma_{rz}^b\gamma_{rz}+\sigma_{\theta z}^b\gamma_{\theta z}\\-D_r^bE_r-D_\theta^bE_\theta-D_z^bE_z\\-B_r^bH_r-B_\theta^bH_\theta-B_z^bH_z+2m_{r\theta}^b\chi_{r\theta}^b\end{Bmatrix}r\mathrm{dz}\mathrm{d}\theta\mathrm{d}r\\&+\frac{1}{2}\iint_{r\theta}\int_{-\frac{h_c}{2}}^{\frac{h_c}{2}}\left\{\sigma_{rr}^c\varepsilon_{rr}+\sigma_{\theta\theta}^c\varepsilon_{\theta\theta}+\sigma_{r\theta}^c\gamma_{r\theta}+\sigma_{rz}^c\gamma_{rz}+\sigma_{\theta z}^c\gamma_{\theta z}+2m_{r\theta}^c\chi_{r\theta}^c\right\}r\mathrm{dz}\mathrm{d}\theta\mathrm{d}r\\&+\frac{1}{2}\iint_{r\theta}\int_{\frac{h_c}{2}}^{\frac{h_c}{2}+h_t}\begin{Bmatrix}\sigma_{rr}^t\varepsilon_{rr}+\sigma_{\theta\theta}^t\varepsilon_{\theta\theta}+\sigma_{r\theta}^t\gamma_{r\theta}+\sigma_{rz}^t\gamma_{rz}+\sigma_{\theta z}^t\gamma_{\theta z}\\-D_r^tE_r-D_\theta^tE_\theta-D_z^tE_z\\-B_r^tH_r-B_\theta^tH_\theta-B_z^tH_z+2m_{r\theta}^t\chi_{r\theta}^t\end{Bmatrix}r\mathrm{dz}\mathrm{d}\theta\mathrm{d}r=0\end{aligned} \tag{48}$$

Replacing the strain-displacement relations and defining the stress resultants, variations of strain energy can be achieved as

$$\delta U=\iint_{r\theta}\begin{bmatrix}\left(-\frac{\partial}{\partial r}(rN_{rr})+N_{\theta\theta}-\frac{\partial}{\partial\theta}(N_{r\theta})\right)\delta u_0\\+\left(-\frac{\partial}{\partial\theta}(N_{\theta\theta})-N_{r\theta}-\frac{\partial}{\partial r}(rN_{r\theta})\right)\delta v_0\\+\left(-\frac{\partial}{\partial r}(rQ_r)-\frac{\partial}{\partial\theta}(Q_\theta)-\frac{1}{2}\frac{\partial^2}{\partial r^2}(rY_{r\theta})-\frac{1}{2}\frac{\partial}{\partial r}(Y_{r\theta})\right)\delta w_0\\+\left(-\frac{\partial}{\partial r}(rM_{rr})+M_{\theta\theta}+rQ_r-\frac{\partial}{\partial\theta}(M_{r\theta})-\frac{1}{2}\frac{\partial}{\partial r}(rY_{r\theta})-\frac{1}{2}(Y_{r\theta})\right)\delta\lambda_r\\+\left(-M_{r\theta}-\frac{\partial}{\partial\theta}(M_{\theta\theta})-\frac{\partial}{\partial r}(rM_{r\theta})+rQ_\theta\right)\delta\lambda_\theta\\+\left(\frac{\partial}{\partial r}(r\bar{D}_r)+\frac{\partial}{\partial\theta}(\bar{D}_\theta)+r\bar{D}_z\right)\delta\phi\\+\left(\frac{\partial}{\partial r}(r\bar{B}_r)+\frac{\partial}{\partial\theta}(\bar{B}_\theta)+r\bar{B}_z\right)\delta\psi\end{bmatrix}\mathrm{d}\theta\,\mathrm{d}r \tag{49}$$

in which the used resultants in Eq. (49) are as follow

$$\begin{aligned}&\{N_{rr},M_{rr}\}=\int_{-\frac{h_c}{2}-h_b}^{-\frac{h_c}{2}}\{1,\,z\}\sigma_{rr}^b\,\mathrm{dz}+\int_{-\frac{h_c}{2}}^{\frac{h_c}{2}}\{1,\,z\}\sigma_{rr}^c\,\mathrm{dz}+\int_{\frac{h_c}{2}}^{\frac{h_c}{2}+h_t}\{1,\,z\}\sigma_{rr}^t\,\mathrm{dz},\\&\{N_{r\theta},M_{r\theta}\}=\int_{-\frac{h_c}{2}-h_b}^{-\frac{h_c}{2}}\{1,\,z\}\sigma_{r\theta}^b\,\mathrm{dz}+\int_{-\frac{h_c}{2}}^{\frac{h_c}{2}}\{1,\,z\}\sigma_{r\theta}^c\,\mathrm{dz}+\int_{\frac{h_c}{2}}^{\frac{h_c}{2}+h_t}\{1,\,z\}\sigma_{r\theta}^t\,\mathrm{dz},\\&\{N_{\theta\theta},M_{\theta\theta}\}=\int_{-\frac{h_c}{2}-h_b}^{-\frac{h_c}{2}}\{1,\,z\}\sigma_{\theta\theta}^b\,\mathrm{dz}+\int_{-\frac{h_c}{2}}^{\frac{h_c}{2}}\{1,\,z\}\sigma_{\theta\theta}^c\,\mathrm{dz}+\int_{\frac{h_c}{2}}^{\frac{h_c}{2}+h_t}\{1,\,z\}\sigma_{\theta\theta}^t\,\mathrm{dz},\\&\{Q_r,\,Q_\theta\}=\int_{-\frac{h_c}{2}-h_b}^{-\frac{h_c}{2}}\left\{\sigma_{rz}^b,\,\sigma_{\theta z}^b\right\}\mathrm{dz}+\int_{-\frac{h_c}{2}}^{\frac{h_c}{2}}\left\{\sigma_{rz}^c,\,\sigma_{\theta z}^c\right\}\mathrm{dz}+\int_{\frac{h_c}{2}}^{\frac{h_c}{2}+h_t}\left\{\sigma_{rz}^t,\,\sigma_{\theta z}^t\right\}\mathrm{dz},\\&Y_{r\theta}=\int_{-\frac{h_c}{2}-h_b}^{-\frac{h_c}{2}}m_{r\theta}^b\,\mathrm{dz}+\int_{-\frac{h_c}{2}}^{\frac{h_c}{2}}m_{r\theta}^c\,\mathrm{dz}+\int_{\frac{h_c}{2}}^{\frac{h_c}{2}+h_t}m_{r\theta}^t\,\mathrm{dz},\\&\left\{\bar{B}_r,\,\bar{B}_\theta\right\}=\int_{-\frac{h_c}{2}-h_b}^{-\frac{h_c}{2}}\{B_r,\,B_\theta\}\cos\left(\frac{\pi z_b}{h_b}\right)\mathrm{dz}+\int_{\frac{h_c}{2}}^{\frac{h_c}{2}+h_t}\{B_r,\,B_\theta\}\cos\left(\frac{\pi z_t}{h_t}\right)\mathrm{dz},\\&\bar{B}_z=\int_{-\frac{h_c}{2}-h_b}^{-\frac{h_c}{2}}B_z\left[\frac{\pi}{h_b}\right]\sin\left(\frac{\pi z_b}{h_b}\right)\mathrm{dz}+\int_{\frac{h_c}{2}}^{\frac{h_c}{2}+h_t}B_z\left[\frac{\pi}{h_t}\right]\sin\left(\frac{\pi z_t}{h_t}\right)\mathrm{dz},\\&\left\{\bar{D}_r,\,\bar{D}_\theta\right\}=\int_{-\frac{h_c}{2}-h_b}^{-\frac{h_c}{2}}\{D_r,\,D_\theta\}\cos\left(\frac{\pi z_b}{h_b}\right)\mathrm{dz}+\int_{\frac{h_c}{2}}^{\frac{h_c}{2}+h_t}\{D_r,\,D_\theta\}\cos\left(\frac{\pi z_t}{h_t}\right)\mathrm{dz},\\&\bar{D}_z=\int_{-\frac{h_c}{2}-h_b}^{-\frac{h_c}{2}}D_z\left[\frac{\pi}{h_b}\right]\sin\left(\frac{\pi z_b}{h_b}\right)\mathrm{dz}+\int_{\frac{h_c}{2}}^{\frac{h_c}{2}+h_t}D_z\left[\frac{\pi}{h_t}\right]\sin\left(\frac{\pi z_t}{h_t}\right)\mathrm{dz}\end{aligned} \tag{50}$$

in which

$$\begin{aligned}z_b&=z+\frac{h_c}{2}+\frac{h_b}{2},\\z_t&=z-\frac{h_c}{2}-\frac{h_t}{2}\end{aligned} \tag{51}$$

3.2 Kinetic energy

The three-layered micro plate kinetic energy is written as (Ferreira *et al*. 2008)

$$\begin{aligned}K=&\frac{1}{2}\iint_{r\theta}\int_{-\frac{h_c}{2}-h_b}^{-\frac{h_c}{2}}\rho(z)\left(\left(\frac{\partial u}{\partial t}\right)^2+\left(\frac{\partial v}{\partial t}\right)^2+\left(\frac{\partial w}{\partial t}\right)^2\right)r\mathrm{dz}\mathrm{d}\theta\mathrm{d}r\\&+\frac{1}{2}\iint_{r\theta}\int_{-\frac{h_c}{2}}^{\frac{h_c}{2}}\rho(z)\left(\left(\frac{\partial u}{\partial t}\right)^2+\left(\frac{\partial v}{\partial t}\right)^2+\left(\frac{\partial w}{\partial t}\right)^2\right)r\mathrm{dz}\mathrm{d}\theta\mathrm{d}r\\&+\frac{1}{2}\iint_{r\theta}\int_{\frac{h_c}{2}}^{\frac{h_c}{2}+h_t}\rho(z)\left(\left(\frac{\partial u}{\partial t}\right)^2+\left(\frac{\partial v}{\partial t}\right)^2+\left(\frac{\partial w}{\partial t}\right)^2\right)r\mathrm{dz}\mathrm{d}\theta\mathrm{d}r\end{aligned} \tag{52}$$

Inserting displacements from Eq. (7) into Eq. (52), the variations of kinetic energy is determined as

$$\int_{t_1}^{t_2}\delta K\ \mathrm{dt}=\int_{t_1}^{t_2}\iiint\begin{pmatrix} rI_0\frac{\partial u_0}{\partial t}\frac{\partial \delta u_0}{\partial t}+rI_1\frac{\partial u_0}{\partial t}\frac{\partial \delta \varphi_r}{\partial t}\\ +rI_1\frac{\partial \lambda_r}{\partial t}\frac{\partial \delta u_0}{\partial t}+rI_2\frac{\partial \lambda_r}{\partial t}\frac{\partial \delta \lambda_r}{\partial t}\\ +rI_0\frac{\partial v_0}{\partial t}\frac{\partial \delta v_0}{\partial t}+rI_1\frac{\partial v_0}{\partial t}\frac{\partial \delta \lambda_\theta}{\partial t}\\ +rI_1\frac{\partial \lambda_\theta}{\partial t}\frac{\partial \delta v_0}{\partial t}+rI_2\frac{\partial \lambda_\theta}{\partial t}\frac{\partial \delta \lambda_\theta}{\partial t}\\ +rI_0\frac{\partial w_0}{\partial t}\frac{\partial \delta w_0}{\partial t}\end{pmatrix}\mathrm{drd\theta dt} \tag{53}$$

Therefore

$$\int_{t_1}^{t_2}\delta K\ \mathrm{dt}=\int_{t_1}^{t_2}\iiint\begin{pmatrix}\left[-\frac{\partial}{\partial t}(rI_0\frac{\partial u_0}{\partial t})-\frac{\partial}{\partial t}(rI_1\frac{\partial \lambda_r}{\partial t})\right]\delta u_0\\ +\left[-\frac{\partial}{\partial t}(rI_0\frac{\partial v_0}{\partial t})-\frac{\partial}{\partial t}(rI_1\frac{\partial \lambda_\theta}{\partial t})\right]\delta v_0\\ ?-\left[\frac{\partial}{\partial t}\ rI_0\frac{\partial w_0}{\partial t})\right]\delta w_0\\ +\left[-\frac{\partial}{\partial t}(rI_1\frac{\partial u_0}{\partial t})-\frac{\partial}{\partial t}(rI_2\frac{\partial \lambda_r}{\partial t})\right]\delta \lambda_r\\ +\left[-\frac{\partial}{\partial t}(rI_1\frac{\partial v_0}{\partial t})-\frac{\partial}{\partial t}(rI_2\frac{\partial \lambda_\theta}{\partial t})\right]\delta \lambda_\theta\end{pmatrix}\mathrm{drd\theta dt} \tag{54}$$

in which

$$\begin{aligned} I_i=&\int_{-\frac{h_c}{2}-h_b}^{-\frac{h_c}{2}}\rho(z)\,z^i\ \mathrm{dz}+\int_{-\frac{h_c}{2}}^{\frac{h_c}{2}}\rho(z)\,z^i\ \mathrm{dz}\\ &+\int_{\frac{h_c}{2}}^{\frac{h_c}{2}+h_t}\rho(z)\,z^i\ \mathrm{dz},\qquad i=0,1,2\end{aligned} \tag{55}$$

3.3 External work

The external work in the current study includes two sectors: the first one due to the Pasternak elastic foundation and the second one for magneto electro-mechanical pre loads. So

$$W_{ext}=W_{foundation}+W_{preloads} \tag{56}$$

The force of elastic foundation can be written as (Duc 2013, Arefi *et al.* 2018)

$$f_{foundation}=rK_W w(r,\theta,t)-rK_G\nabla^2 w(r,\theta,t) \tag{57}$$

Spring and shear layer constants are shown by K_W and K_G, respectively. Therefore, the work of foundation force can be calculated using the below relation (Ebrahimi *et al.* 2017b, Yazid *et al.* 2018)

$$W_{foundation}=\frac{1}{2}\int_r\int_\theta\ \left[-f_{foundation}\ w(r,\theta,t)\right]r\ \mathrm{dr\,d\theta} \tag{58}$$

The work of pre loads can be achieved using the following equation as (Meirovitch 1997)

$$W_{preloads}=\frac{1}{2}\int_r\int_\theta\ \left[N_r^{ext}\left(\frac{\partial w}{\partial r}\right)^2+\frac{1}{r^2}N_\theta^{ext}\left(\frac{\partial w}{\partial \theta}\right)^2\right]r\ \mathrm{dr\,d\theta} \tag{59}$$

in which N_r^{ext} and N_θ^{ext} are the external forces in the radial and tangential directions and are consist of mechanical, electrical and magnetic loads as follows

$$N_r^{ext}=N_r^M+N_r^E+N_r^H, \tag{60}$$

$$N_\theta^{ext}=N_\theta^M+N_\theta^E+N_\theta^H \tag{61}$$

where the multi-physical loads are defined as

$$N_r^M=P_0,\qquad N_r^E=-2e_{31}\phi_0,\qquad N_r^H=-2q_{31}\psi_0, \tag{62}$$

$$N_\theta^M=P_0,\qquad N_\theta^E=-2e_{32}\phi_0,\qquad N_\theta^H=-2q_{32}\psi_0 \tag{63}$$

in which P_0 is the mechanical pre load.

3.4 Hamilton's principle

Hamilton's principle is employed in the present research to obtain motion equations as follow (Amir 2016, Sidhoum *et al.* 2018):

$$\int_{t_1}^{t_2}\left[\delta U-\delta K-\delta W_{ext}\right]\mathrm{dt}=0 \tag{64}$$

where δU and δK represent the variation of strain and kinetic energies, and δW_{ext} is external work variation.

3.5 Governing motion equations

Using Eqs. (49), (54) and (59), substituting in Hamilton's principle and by the assumption of axial symmetric which makes the equations simpler and vanished some terms, the equations are achieved as follow

δu:

$$\begin{aligned} &P_1 r\frac{\partial^2 u}{\partial r^2}+P_1\frac{\partial u}{\partial r}-P_2\frac{1}{r}u+P_3 r\frac{\partial^2 \lambda_r}{\partial r^2}+P_3\frac{\partial \lambda_r}{\partial r}-P_4\frac{1}{r}\lambda_r\\ &+E_1 r\frac{\partial \phi}{\partial r}+(E_1-E_2)\phi+H_1 r\frac{\partial \psi}{\partial r}+(H_1-H_2)\psi\\ &-I_0 r\frac{\partial^2 u}{\partial t^2}-I_1 r\frac{\partial^2 \lambda_r}{\partial t^2}=0\end{aligned} \tag{65}$$

δw:

$$\begin{aligned} &-\frac{1}{4}rl_m^2P_5\frac{\partial^4 w}{\partial r^4}-\frac{1}{2}l_m^2P_5\frac{\partial^3 w}{\partial r^3}+\left(\frac{1}{4}\frac{l_m^2}{r}P_5-r\left(K_G-N_r^{ext}\right)+r\kappa_f P_5\right)\frac{\partial^2 w}{\partial r^2}\\ &+\left(-\frac{1}{4}\frac{l_m^2}{r^2}P_5-\left(K_G-N_r^{ext}\right)+\kappa_f P_5\right)\frac{\partial w}{\partial r}+rK_W w+\frac{1}{4}rl_m^2P_5\frac{\partial^3 \lambda_r}{\partial r^3}\\ &+\left(\frac{1}{2}l_m^2P_5\right)\frac{\partial^2 \lambda_r}{\partial r^2}+\left(r\kappa_f P_5-\frac{1}{4}\frac{l_m^2}{r}P_5\right)\frac{\partial \lambda_r}{\partial r}+\left(\kappa_f P_5+\frac{1}{4}\frac{l_m^2}{r^2}P_5\right)\lambda_r\\ &-r\kappa_f E_3\frac{\partial^2 \phi}{\partial r^2}-\kappa_f E_3\frac{\partial \phi}{\partial r}-r\kappa_f H_3\frac{\partial^2 \psi}{\partial r^2}-\kappa_f H_3\frac{\partial \psi}{\partial r}-rI_0\frac{\partial^2 w}{\partial t^2}=0\end{aligned} \tag{66}$$

$\delta\lambda_r$:

$$\begin{aligned} &P_3 r\frac{\partial^2 u}{\partial r^2}+P_3\frac{\partial u}{\partial r}-P_4\frac{1}{r}u-\frac{1}{4}rl_m^2P_5\frac{\partial^3 w}{\partial r^3}-\frac{1}{4}l_m^2P_5\frac{\partial^2 w}{\partial r^2}+\left(\frac{1}{4}\frac{l_m^2}{r}P_5-r\kappa_f P_5\right)\frac{\partial w}{\partial r}\\ &+\left(\frac{1}{4}rl_m^2P_5+P_6 r\right)\frac{\partial^2 \lambda_r}{\partial r^2}+\left(\frac{1}{4}l_m^2P_5+P_6\right)\frac{\partial \lambda_r}{\partial r}-\left(\frac{1}{4}\frac{l_m^2}{r}P_5+r\kappa_f P_5+P_7\frac{1}{r}\right)\lambda_r\\ &+\left(\kappa_f E_3+E_4\right)r\frac{\partial \phi}{\partial r}+(E_4-E_5)\phi+\left(\kappa_f H_3+H_4\right)r\frac{\partial \psi}{\partial r}+(H_4-H_5)\psi\\ &-I_1 r\frac{\partial^2 u}{\partial t^2}-I_2 r\frac{\partial^2 \lambda_r}{\partial t^2}=0\end{aligned} \tag{67}$$

$\delta\phi$:

$$E_1 r\frac{\partial u}{\partial r}+E_2 u+E_3 r\frac{\partial^2 w}{\partial r^2}+E_3\frac{\partial w}{\partial r}+\left(E_3+E_4\right)r\frac{\partial \lambda_r}{\partial r}+\left(E_3+E_5\right)\lambda_r+E_6 r\frac{\partial^2\phi}{\partial r^2}+E_6\frac{\partial\phi}{\partial r}-E_7 r\phi+H_6 r\frac{\partial^2\psi}{\partial r^2}+H_6\frac{\partial\psi}{\partial r}-H_7 r\psi=0 \quad (68)$$

$\delta\psi$:

$$H_1 r\frac{\partial u}{\partial r}+H_2 u+H_3 r\frac{\partial^2 w}{\partial r^2}+H_3\frac{\partial w}{\partial r}+\left(H_3+H_4\right)r\frac{\partial \lambda_r}{\partial r}+\left(H_3+H_5\right)\lambda_r+H_6 r\frac{\partial^2\phi}{\partial r^2}+H_6\frac{\partial\phi}{\partial r}-H_7 r\phi+R_1 r\frac{\partial^2\psi}{\partial r^2}+R_1\frac{\partial\psi}{\partial r}-R_2 r\psi=0 \quad (69)$$

where the used coefficients in the governing motion equations are defined in the "Appendix" section.

3.6 Boundary and continuity conditions

The boundary and continuity conditions of the annular and circular micro plate are presented in the following. It is noteworthy that the classical (macro) plate needs five conditions at each outer and inner edges (Reddy *et al.* 1999), while the micro plate needs one more condition.

3.6.1 Circular plate

For the circular micro plates, at the center of the plate, the continuity condition should be established. To this purpose the following relations are used

$$u=0,\qquad \lambda_r=0,\qquad \frac{\partial w}{\partial r}=0,\qquad \frac{\partial}{\partial r}(rY_{r\theta})+Y_{r\theta}=0,\qquad \phi=0,\qquad \psi=0 \quad (70)$$

and for the edges of the micro plate, depends on the type of boundary condition, their relations are ruling as:

(a) Clamped edges

$$u=0,\qquad w=0,\qquad \lambda_r=0,\qquad \frac{\partial w}{\partial r}=0\ ,\qquad \phi=0,\qquad \psi=0 \quad (71)$$

(b) Simply supported edges

$$u=0,\qquad w=0,\qquad Y_{r\theta}=0,\qquad M_{rr}=0,\qquad \phi=0,\qquad \psi=0 \quad (72)$$

3.6.2 Annular plate

The boundary conditions of the annular micro plate can be one of the clamped or simply supported type in edges of the plate. Noted that the boundary conditions of the annular plates are expressed using two letters: the first letter describes the condition of the inner edge and the second one is related to the outer edge. For example, C-S refers to the inner clamped and outer simply supported edges.

4. Solution procedure

Among the various methods to solve the differential equations, GDQM is selected in the present study as an accurate method. In addition by comparison with other numerical methods such as Galerkin or FEM, it can be found that convergence of the GDQM occurs earlier than the others (Malekzadeh and Zarei 2014). The general idea of the GDQ method is based on estimating the derivative of a function relative to a variable at a point by a linear combination of the weighted values of the function at all points in the direction of that variable. As a first step to use this method, the problem domain must be discrete. Then the weighting coefficients should be calculated based on the discrete points.

Distribution of grid points is important in determining the convergence rate and stability of the GDQM. The optimal distribution of points depends on the degree of derivation in boundary conditions and the number of used points. In this section, the discretization method in the form of a single-variable function is explained. Consider the single- variable function *f(r)* in the domain $a < r < b$. Different methods are available for discretization of the domain. Based on *Chebyshev* polynomial, the points in the domain of problem in radius direction can be distributed as follow (Bert and Malik 1996)

$$R_i=b+\left(\frac{a-b}{2}\right)\left\{1-\cos\frac{(i-1)\pi}{(N-1)}\right\},\qquad i=1,2,...,N \quad (73)$$

where N represents the number of points, b and a are the inner and outer radii, respectively.

According to GDQ method, the derivative of the *m-th* order function *f(r)* at point r_i is equal to (Liew *et al*. 1996)

$$f^{(m)}(r_i)=\sum_{j=1}^{N}C_{ij}^{(m)}f(r_j),\qquad i=1,2,\ldots,N \quad (74)$$

in which $C_{ij}^{(m)}$ is the weighting coefficient of the GDQM. To determine these weighting coefficients, Lagrange interpolation polynomials are used as (Tohidi *et al.* 2018)

$$g_j(r)=\frac{M(r)}{(r-r_j)M^{(1)}(r_j)} \quad (75)$$

where

$$M(r)=\prod_{k=1}^{N}(r-r_k);\qquad M^{(1)}(r_j)=\prod_{k=1,k\neq j}^{N}r_j-r_k \quad (76)$$

That $M^{(1)}(r)$ is the first-order derivative of $M(r)$. The first-order derivative weighting coefficients are derived from the below relation (Shu 2012)

$$C_{ij}^{(1)}=\begin{cases}g_j^{(1)}(r_i) & j\neq i\\ -\sum_{j=1,j\neq i}^{N}C_{ij}^{(1)} & j=i\end{cases}\qquad i,j=1,2,\ldots,N \quad (77)$$

The higher order weighting coefficients will be calculated using the following equation

$$C_{ij}^{(m)}=\begin{cases} n\left(C_{ij}^{(1)}C_{ii}^{(m-1)}-\dfrac{C_{ij}^{(m-1)}}{r_i-r_j}\right) & j\neq i \\ -\sum\limits_{j=1,j\neq i}^{N}C_{ij}^{(m)} & j=i \end{cases} \qquad i,j=1,2,\ldots,N \tag{78}$$

Using the GDQ relations and by converting the motion and boundary conditions equations to the following for, natural frequencies of the structure can be obtained

$$\left(\left[K\right]-\omega^2\left[M\right]\right)\left\{d\right\}=0 \tag{79}$$

where $\{d\}$ represents the displacements vector. Solving the eigenvalue problem of Eq. (79), leads to obtaining the frequencies.

5. Numerical results and discussion

5.1 Convergence of the results

As stated in the previous section, rapid convergence is one of the featured features of the GDQM. So, in the present section, the convergence of the results respect to the number of grid points is considered. Tables 1 and 2 are presented the results of the circular and annular micro plates, respectively for different boundary conditions with regard to variation of grid point's number. It should be noted that these tables are presented for the non-symmetric porosity distribution of porous core and uniform CNTs distribution of CNTRCs face sheets.

It is found that the convergence occurs rapidly for both types of considering plate with about 15 points. So, all the other results in tables and figures are obtained based on 19 points.

Table 1 Convergence of the fundamental natural frequency of circular plate

N	Boundary Condition	
	Clamped ($\times10^6$)	Simply supported ($\times10^7$)
5	4.3715	1.2754
7	3.4104	0.1298
9	3.1319	0.1304
11	3.0083	0.1255
13	2.9468	0.1214
15	2.9123	0.1185
17	2.8905	0.1163
19	2.8752	0.1146
21	2.8639	0.1134
23	2.8549	0.1124
25	2.8484	0.1116

Table 2 Convergence of the fundamental natural frequency for various boundary conditions of annular plate

N	Boundary Condition			
	C-C ($\times10^7$)	S-C ($\times10^7$)	C-S ($\times10^7$)	S-S ($\times10^7$)
5	1.5958	2.2666	0.6466	1.5484
7	1.4835	1.2691	1.1061	1.3286
9	1.4530	1.2516	1.1079	0.9457
11	1.4492	1.2493	1.1106	0.9459
13	1.4488	1.2490	1.1113	0.9460
15	1.4488	1.2490	1.1114	0.9460
17	1.4488	1.2490	1.1114	0.9459
19	1.4488	1.2490	1.1114	0.9459
21	1.4488	1.2490	1.1114	0.9460
23	1.4488	1.2490	1.1115	0.9459
25	1.4488	1.2490	1.1115	0.9459

5.2 Validation of the results

To validate the formulation and solution process, the results for the simpler states are considered. Table 3 presents the dimensionless fundamental frequency of an isotropic circular macro plate and is compared the results with the previous studies (Lal and Ahlawat 2015, Leissa 1969, Wu *et al.* 2002, Zhou *et al.* 2003). So, by neglecting small scale parameter, magneto electro fields and in absence of an elastic foundation for a single-layered isotropic homogenous plate, the results are obtained. The dimensionless frequency for this table is defined as $\Omega=\omega a\sqrt{\rho h/P_1}$ and v=0.3. Results are in good convergence with the other studies and the little difference between the results can be caused by the different used theories. The other studies used CPT while the present one is based on FSDT.

Table 3 Comparison of the present results with previous ones for circular macro plate

Mode Number		Boundary Condition	
		Clamped	Simply supported
1	Zhou *et al.* (2003)	10.216	4.9352
	Leissa (1969)	10.216	-
	Lal and Ahlawat (2015)	10.2158	4.9351
	Wu *et al.* (2002)	10.216	4.935
	Present	10.2142	4.9417
2	Zhou *et al*. (2003)	39.771	29.720
	Leissa (1969)	39.771	-
	Lal and Ahlawat (2015)	39.7711	29.7200
	Wu *et al.* (2002)	39.771	29.720
	Present	39.4166	29.5847

Table 4 Comparison of the present results with other studies for annular macro plate

Boundary Condition	Results			
	Chakraverty *et al.* (2001)	Zhou *et al.* (2011) (Ansys)	Zhou *et al.* (2011) (Analytical)	Present
C-C	61.88	61.70	61.872	61.7365
S-C	44.93	44.982	44.932	45.7028
C-S	41.27	41.155	41.261	40.6689
S-S	28.08	28.127	28.184	28.2904

Table 5 Comparing the natural frequencies of the first three modes of isotropic homogenous annular micro plate (h/l_m=2)

Boundary Condition	Mode Number	Results	
		Ke *et al.* (2012)	Present
C-C	**1**	3.9901	3.9975
	2	6.3932	6.3932
	3	8.9566	9.0274
S-S	**1**	2.3169	2.3184
	2	6.3932	6.3932
	3	7.2014	7.2032

Table 4 is considered the dimensionless natural frequency of the first mode of the isotropic homogenous macro annular plate for the various boundary conditions. The non-dimensional frequency is defined the same as Table 3, the Poisson's ratio is equal to 1/3 and ratio of the inner to the outer radius is 0.4. These results are also in good agreement with the previous ones (Chakraverty *et al*. 2001, Zhou *et al*. 2011).

At the final step to examine the reliability of the results, the natural frequencies of first three modes of micro annular plate which is isotropic homogenous and single-layer are considered and are presented in Table 5. Similar to the previous results, it shows the excellent agreement between the present results and those reported by Ke *et al.* (2012).

5.3 Parametric study

Now the results for the MEE vibration analysis of circular/ annular micro sandwich plates with saturated porous core and FG-CNTRCs face sheets subjected to magneto- electro-mechanical pre loads are presented and effect of different parameters such as pores distribution in core, porosity coefficient, pores compressibility, CNTs distribution in face sheets, volume fraction of CNTs, foundation parameters, multi-physical pre loads and geometric size of the annular and circular plates are investigated. As stated before, the face sheets are made from PVDF as the matrix and SWCNTs as the reinforcements. The material properties of the SWCNTs and PVDF are presented in Table 6 and the efficiency parameters of CNTs are in Table 7.

Table 6 Material properties of the CNTRCs face sheets (Amir *et al*. 2018a)

Properties	SWCNTs	PVDF
v	0.175	0.34
ρ (kg/m^3)	1400	1780
e_{31} (C/m^2)	0	-0.13
e_{32} (C/m^2)	0	-0.145
e_{15} (C/m^2)	0	-0.135
q_{31} (N/Am)	22	0
d_{33} (Ns/CV)	0	-46
μ_{33} (Ns^2/C^2)	0.25	-46
s_{11} (nF/m^2)	0	0.1107
s_{33} (nF/m^2)	0	0.1061
	E_{11} (TPa)= 5.6466	E_m (GPa)= 2.2
	E_{22} (TPa) 7.0800	
	G_{12} (TPa)= 1.9445	

Table 7 Efficiency parameters of CNTs (Amir *et al*. 2018a)

V^*_{CNT}	η_1	η_2	η_3
0.12	0.137	1.022	0.715
0.17	0.142	1.626	1.138
0.28	0.141	1.585	1.109

It should be noted that the Tennessee marble is selected as the porous core with Young's elasticity modulus equal to 60 *GPa*, density 2700 kg/m^3, and its Poisson's ratio is 0.25.

Fig. 3 depicts the effect of porosity variations on the fundamental frequency of the annular micro plate. The non-symmetric pores distribution type is selected for the core and CNTs are distributed uniformly through the face sheets thickness. Results are shown for various boundary conditions i.e., C-C, C-S, S-C, and S-S. As it can be seen in this figure, increasing the porosity coefficient which shows the ratio of void to bulk volume, the frequency decreases. Also as it can be expected the frequency of both edges clamped plate is more than the other conditions. Generally, the clamped condition raises the stiffness and stability of the plate and as the plate becomes stiffer, its vibrations will be reduced and natural frequency will be increased.

Fig. 4 shows the effect of porosity increasing for three considering porosity distributions. Similar to Fig. 3, increasing the porosity decreases the frequency. The frequency of symmetric distribution is more than two other types. The natural frequency is related to the root square of stiffness to mass ratio and for the symmetric distribution, the rate of decreasing of this ratio is less than symmetric and monotonous pores distribution. For Figs. 3 and 4 the following specifications are used: B=0.1, b=0.1μm, a=5b, h_c=a/6, l_m=h_c/2, h_t=h_b=h_c/10 and volume fraction of CNTs equals to 0.17.

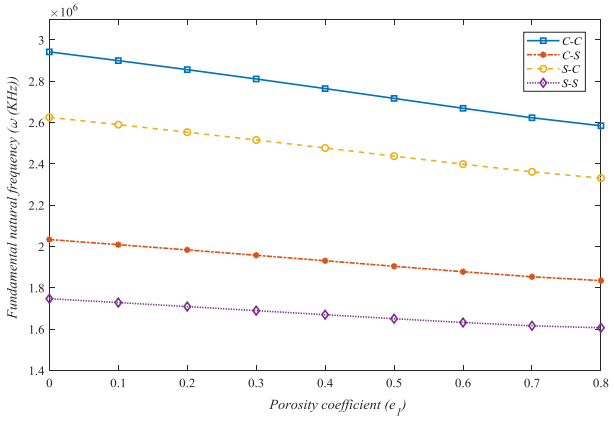

Fig. 3 Comparison of the various boundary conditions of the annular plate

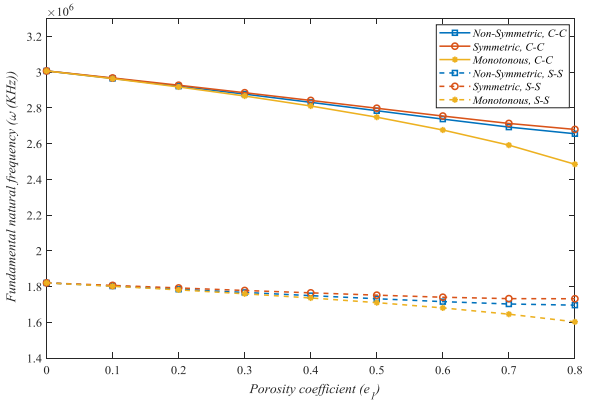

Fig. 4 Effect of porosity variations on the fundamental frequency of the annular plate

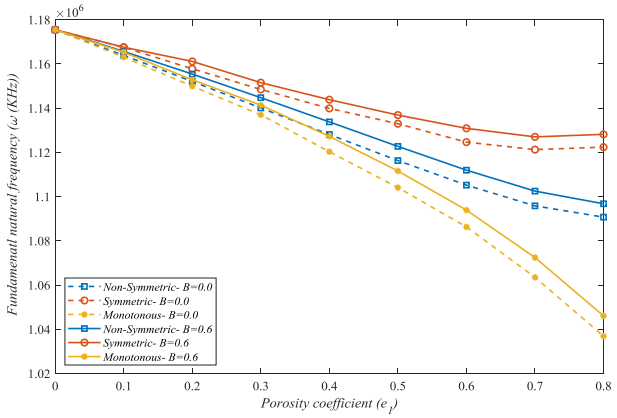

Fig. 5 Investigation the pores distributions and compressibility on the fundamental frequency of the circular clamped plate

Table 8 Effect of pores compressibility on the fundamental natural frequency of the annular plate

	C-C				
	B				
	0	**0.2**	**0.4**	**0.6**	**0.8**
	Non-symmetric distribution				
ω_1 (GHz)	2.8764	2.8780	2.8795	2.8810	2.8824
	Symmetric distribution				
ω_1 (GHz)	2.8845	2.8855	2.8864	2.8874	2.8884
	Monotonous distribution				
ω_1 (GHz)	2.8657	2.8676	2.8693	2.8710	2.8726
	S-S				
	Non-symmetric distribution				
ω_1 (GHz)	1.7661	1.7687	1.7711	1.7736	1.7759
	Symmetric distribution				
ω_1 (GHz)	1.7779	1.7797	1.7804	1.7832	1.7852
	Monotonous distribution				
ω_1 (GHz)	1.7587	1.7623	1.7654	1.7677	1.7693

The effect of pores compressibility which is shown by Skempton coefficient *B* is investigated in Table 8. This table shows by increasing pores compressibility the plate becomes stiffer and its stability increases, so its frequency increases slightly. This effect is considered for C-C and S-S micro annular plate and for three types of porosity distributions.

The effect of Skempton and porosity coefficients for the micro circular plate is considered in Fig. 5. Effects of these parameters on the fundamental frequency are similar to the annular plate. For this figure, e_1=0.3 is used.

Table 9 and Figs. 6-7 show the effect of different CNTs distribution in the face sheets for the circular, C-C and S-S annular plates, respectively.

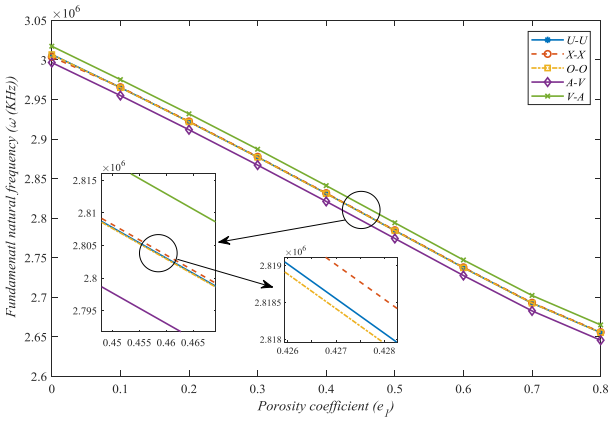

Fig. 6 Effect of various CNTRC face sheets FG types on the fundamental frequency of the annular plate. (C-C)

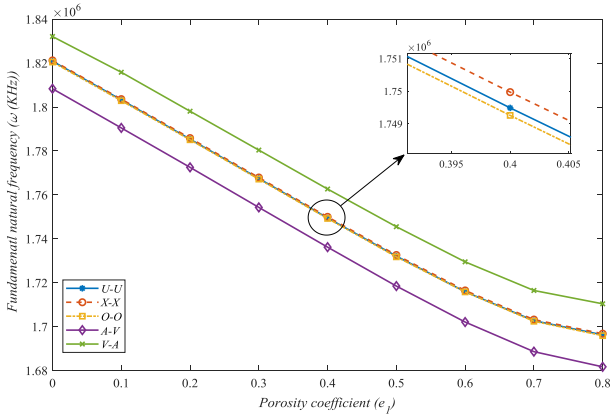

Fig. 7 Effect of various CNTRC face sheets FG types on the fundamental frequency of the annular plate. (S-S)

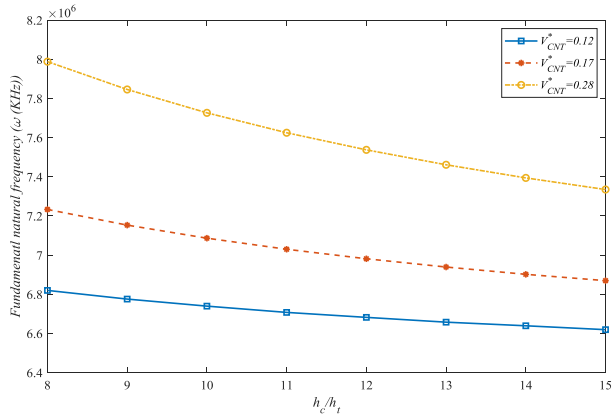

Fig. 8 Effect of CNTs volume fraction variations on the fundamental frequency of the annular plate

Table 9 Various FG types of CNTs distributions effect on the fundamental natural frequency of the clamped circular plate

	e_1						
	0.0	**0.1**	**0.2**	**0.3**	**0.4**	**0.5**	**0.6**
				U-U			
ω_1 (GHz)	1.1754	1.1642	1.1526	1.1409	1.1291	1.1174	1.1064
				FG V-A			
ω_1 (GHz)	1.1831	1.1723	1.1610	1.1494	1.1378	1.1263	1.1155
				FG X-X			
ω_1 (GHz)	1.1757	1.1645	1.1529	1.1412	1.1294	1.1177	1.1067
				FG O-O			
ω_1 (GHz)	1.1752	1.1640	1.1524	1.1407	1.1289	1.1172	1.1062
				FG A-V			
ω_1 (GHz)	1.1680	1.1559	1.1442	1.1323	1.1203	1.1084	1.0971

As it can be seen in Table 9, five different types of FG distribution of CNTs are considered. Maximum and minimum values of the results are for The FG-VA and FG-AV types, respectively. It caused the CNTs in FG-VA are more in the surfaces of the plate rather than the other types.

Increasing volume fraction of the CNTs, enhances the plate's stiffness and the natural frequency will be increased, too. This effect is shown in Fig. 8 for the C-C micro annular plate with non-symmetric core type and uniform CNTs distribution for the face sheets and h_t=h_b=0.1μm.

Effect of the small scale length parameter l_m is presented in Fig. 9 for the circular plate with a=0.5μm and in Table 10 for the annular plate. These data show the effect of total thickness of the plate h which is equal to the sum of three layers thicknesses to the small scale parameter on the fundamental frequency. It can be concluded that by enhancing the small scale parameter, the frequency raises, too.

Core's thickness to the radius of the circular plate ratio variations and its effect on the fundamental frequency of the plate is considered for two clamped and simply supported boundary conditions in Fig. 10. As the core of the sandwich plate becomes thicker, its stiffness increases and consequently its frequency increases too.

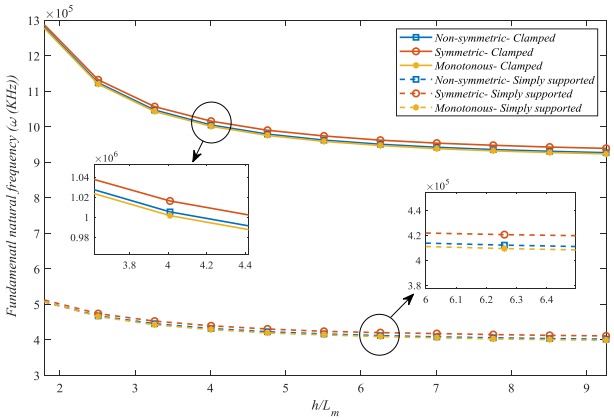

Fig. 9 Size effect on the fundamental frequency of the circular plate

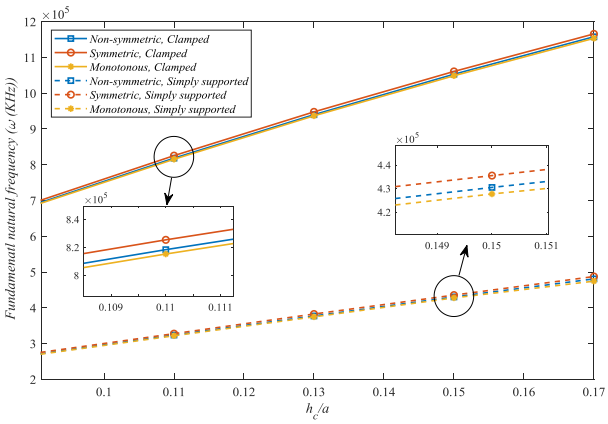

Fig. 10 Effect of core's thickness to plate's radius ratio on the fundamental frequency of the circular plate

Table 10 Size Effect on the fundamental natural frequency of the C-C annular plate

	h/l_m						
	1	**2.5**	**4**	**5.5**	**7**	**8.5**	**10**
	Non-symmetric distribution						
ω_1 (GHz)	4.2230	2.8417	2.555	2.4518	2.4018	2.3736	2.3559
	Symmetric distribution						
ω_1 (GHz)	4.2262	2.8498	2.5663	2.4635	2.4140	2.3859	2.3683
	Monotonous distribution						
ω_1 (GHz)	4.1836	2.8312	2.5462	2.4429	2.3239	2.2650	2.2474

Also, the rate of this increase in clamped condition is more than simply supported one. For this figure, the radius of the circular plate is considered as a=0.5μm.

The effect of aspect ratio of the annular plate is depicted in Fig. 11 for e_1=0.3 and B=0.1. As the outer radius becomes more and by keeping the inner radius constant, the frequency reduces.

Effect of core's to face sheets thickness ratio is considered in Fig. 12. This figure illustrates by increasing the porous core thickness respect to FG-CNTRCs face sheets, due to the much more the stiffness of the face sheets than the core, the plate's stiffness will be reduced and its vibration will be increased. So its frequency will be decreased.

All of the mentioned results were in the absence of the elastic foundation and the effect of Pasternak elastic foundation constants i.e., spring constant K_W and shear layer constant K_G is presented in Figs. 13 and 14. It's clear that by increasing both foundation constant, the natural frequency will be increased. It caused that adding the elastic foundation will increase the stiffness of the structure and based on it, the vibration of the structure reduces. As can be seen in these two figures, the effect of shear layer is more in comparison to spring constant.

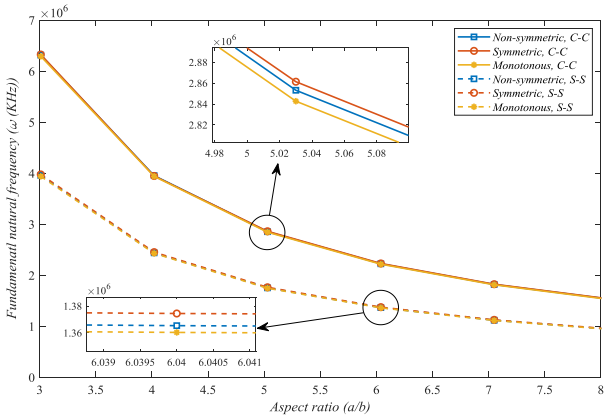

Fig. 11 Effect of aspect ratio on the fundamental frequency of the annular plate

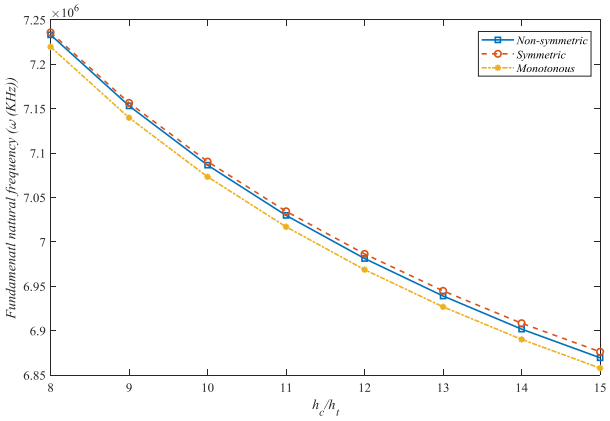

Fig. 12 Effect of core to face sheets thickness ratio on the fundamental frequency of the annular plate

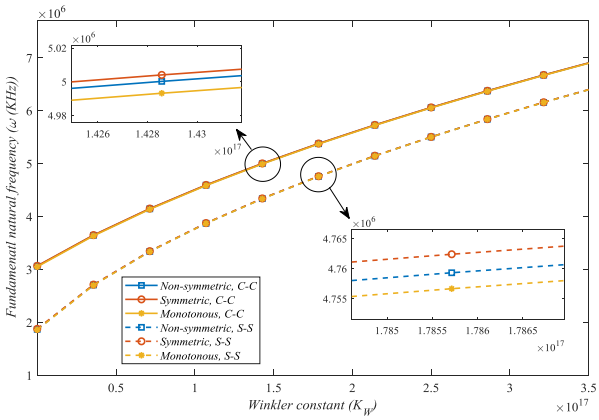

Fig. 13 Effect of Winkler constant of the elastic foundation on the fundamental frequency of the annular plate. (K_G=0)

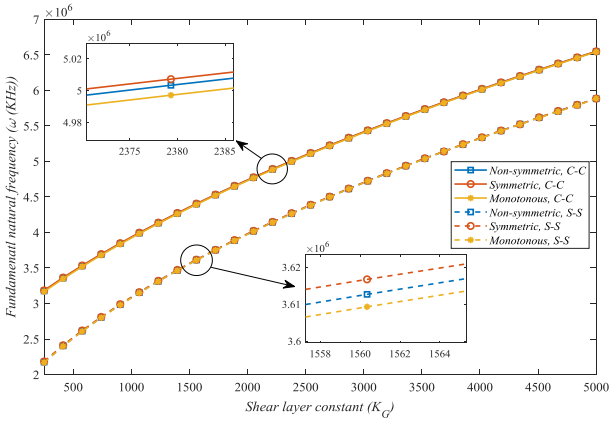

Fig. 14 Effect of shear layer constant of the elastic foundation on the fundamental frequency of the annular plate. (K_W=10^9)

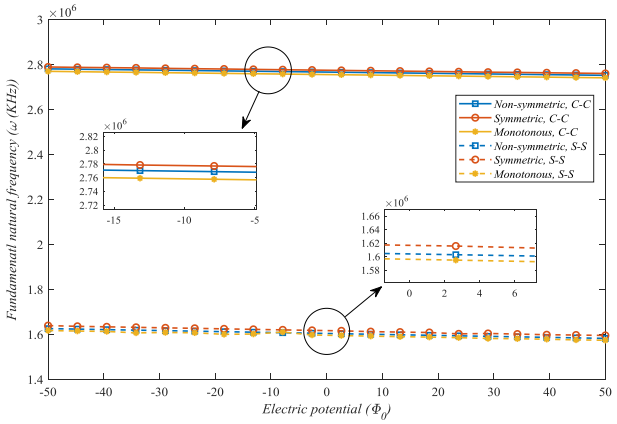

Fig. 15 Effect of electric potential variations on the fundamental frequency of the annular plate

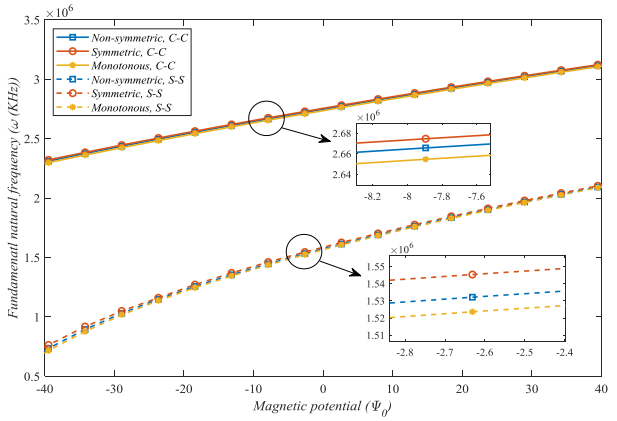

Fig. 16 Effect of magnetic potential variations on the fundamental frequency of the annular plate

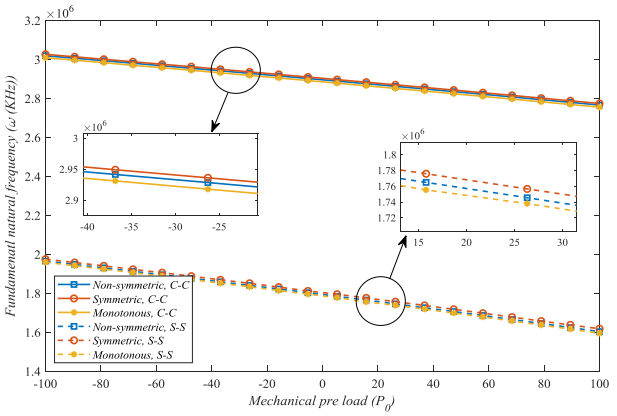

Fig. 17 Effect of mechanical pre load on the fundamental frequency of the annular plate

Effect of multi-physical pre load is presented in Figs. 15-17. Fig. 15 shows the effect of electric potential on the frequency. Increasing the electric potential Φ_0 decreases the frequency slightly.

But the magnetic potential Ψ_0 which its effect on the frequency is shown in Fig. 16 increases the frequency. It's clear that in these figures the symmetric porosity distribution as stated before has the most values of frequencies in comparison two other types.

Fig. 17 demonstrates the effect of tensile and compressive pre mechanical loads P_0 on the natural frequencies and it is concluded that by enhancing it, the frequency will be decreased.

6. Conclusions

Free vibration of three-layered micro annular/ circular plates is analyzed in the current study based on the MCS and FSD theories. The core of the plate was made of saturated porous materials and its face sheets were made of FG-CNTRCs. The matrix of the CNTRCs was PVDF and CNTs were selected as the reinforcement. Pasternak model is used for foundation and multi-physical pre loads are applied to the structure. The attributes of the middle layer were varied through its thickness following the given functions namely non-symmetric, symmetric and monotonous. Hamilton principle and variation formulation were employed to achieve the motion equations and they were solved for various boundary conditions numerically via GDQM which converted them to algebraic equations. Effect of different parameters investigated and concluded that:

- Enhancing the porosity increases the natural frequency.
- The symmetric porosity distribution has the most and monotonous distribution has the least values of the frequencies.
- As the plate becomes more clamped, the frequency increases. Vice versa as the edges of the plate become free, the frequency will be reduced.
- Increasing Skempton coefficient which shows the pores compressibility increases the frequency slightly.
- Among the various CNTs distribution, FG-VA and FG-AV have the most and least values of frequency, respectively.
- Enhancing CNTs volume fraction reduces the vibrations of the structure.
- Increasing small scale length parameter will be caused the plate to vibrate less.
- As the plate's core becomes thicker in comparison to its face sheets, the natural frequency decreases due to its less stiffness in comparison to face sheets.
- By increasing the core's thickness to the radius of the circular plate ratio, the natural frequency will be raised.
- Increasing outer to the inner radius of the annular plate ratio decreases the fundamental frequency.
- Adding the elastic foundation, increases the stiffness of the structure, so the frequency of the sandwich plate will be increased.
- The shear layer constant has more effect rather than spring constant on frequencies of the structure.
- Increasing electric potential and mechanical pre load, decreases the frequency. Vice versa increasing the

magnetic potential will be increased the frequency of the structure.

Acknowledgments

The authors would like to thank the reviewers for their valuable comments and suggestions to improve the clarity of this study.

References

Abdel-Rahman, E.M., Younis, M.I. and Nayfeh, A.H. (2002), "Characterization of the mechanical behavior of an electrically actuated microbeam", *J. Micromech. Microeng.*, **12**(6), 759.

Amir, S. (2016), "Orthotropic patterns of visco-Pasternak foundation in nonlocal vibration of orthotropic graphene sheet under thermo-magnetic fields based on new first-order shear deformation theory", *Proceedings of the Institution of Mechanical Engineers, Part L: Journal of Materials: Design and Applications*, 1464420716670929.

Amir, S., Khorasani, M. and BabaAkbar-Zarei, H. (2018a). "Buckling analysis of nanocomposite sandwich plates with piezoelectric face sheets based on flexoelectricity and first-order shear deformation theory", *J. Sandw. Struct. Mater.*, 109963621879538.

Amir, S., Bidgoli, E.M.R. and Arshid, E. (2018b), "Size-dependent vibration analysis of a three-layered porous rectangular nano plate with piezo-electromagnetic face sheets subjected to pre loads based on SSDT", *Mech. Adv. Mater. Struct.*, 1-15. https://doi.org/10.1080/15376494.2018.1487612.

Arani, A.G., Haghparast, E., Maraghi, Z.K. and Amir, S. (2015), "Static stress analysis of carbon nano-tube reinforced composite (CNTRC) cylinder under non-axisymmetric thermo-mechanical loads and uniform electro-magnetic fields", *Compos. Part B: Eng.*, **68**, 136-145. https://doi.org/10.1016/j.compositesb.2014.08.036

Arefi, M., Bidgoli, E.M.R. and Zenkour, A.M. (2018), "Size-dependent free vibration and dynamic analyses of a sandwich microbeam based on higher-order sinusoidal shear deformation theory and strain gradient theory", *Smart Struct. Syst.*, **22**(1), 27-40. https://doi.org/10.12989/sss.2018.22.1.027.

Arshid, E., Kiani, A. and Amir, S. (2019), "Magneto-electro-elastic vibration of moderately thick FG annular plates subjected to multi physical loads in thermal environment using GDQ method by considering neutral surface", *Proceedings of the Institution of Mechanical Engineers, Part L: Journal of Materials: Design and Applications.*

Arshid, E. and Khorshidvand, A.R. (2017), "Flexural vibrations analysis of saturated porous circular plates using differential auadrature method", *Iranian J. Mech. Eng. T. - ISME*, **19**(1), 78-100.

Arshid, E. and Khorshidvand, A.R. (2018), "Free vibration analysis of saturated porous FG circular plates integrated with piezoelectric actuators via differential quadrature method", *Thin Wall. Struct.*, **125**, 220-233. https://doi.org/10.1016/j.tws.2018.01.007.

Ashrafi, B., Hubert, P. and Vengallatore, S. (2006), "Carbon nanotube-reinforced composites as structural materials for microactuators in microelectromechanical systems", *Nanotechnology*, **17**(19), 4895.

Barati, M.R., Shahverdi, H. and Zenkour, A.M. (2017), "Electro-mechanical vibration of smart piezoelectric FG plates with porosities according to a refined four-variable theory", *Mech. Adv. Mater. Struct.*, **24**(12), 987-998. https://doi.org/10.1080/15376494.2016.1196799.

Bert, C.W. and Malik, M. (1996), "Differential quadrature method in computational mechanics: a review", *Appl. Mech. Rev.*, **49**(1), 1-28.

Biot, M.A. (1964), "Theory of buckling of a porous slab and its thermoelastic analogy", *J. Appl. Mech.*, **31**(2), 194-198. doi:10.1115/1.3629586.

Brush, D.O., Almroth, B.O. and Hutchinson, J.W. (1975), "Buckling of bars, plates, and shells", *J. Appl. Mech.*, **42**, 911.

Bui, T.Q., Do, T. Van, Ton, L.H.T., Doan, D.H., Tanaka, S., Pham, D.T. and Hirose, S. (2016), "On the high temperature mechanical behaviors analysis of heated functionally graded plates using FEM and a new third-order shear deformation plate theory", *Compos.Part B: Eng.*, **92**, 218-241. https://doi.org/10.1016/j.compositesb.2016.02.048.

Bui, T.Q., Nguyen, M.N. and Zhang, C. (2011), "An efficient meshfree method for vibration analysis of laminated composite plates", *Comput. Mech.*, **48**(2), 175-193.

Chakraverty, S., Bhat, R.B. and Stiharu, I. (2001), "Free vibration of annular elliptic plates using boundary characteristic orthogonal polynomials as shape functions in the Rayleigh-Ritz method", *J. Sound Vib.*, **241**, 524-539. doi: 10.1006/jsvi.2000.3243.

Chen, D., Kitipornchai, S. and Yang, J. (2016), "Nonlinear free vibration of shear deformable sandwich beam with a functionally graded porous core", *Thin Wall. Struct.*, **107**, 39-48. https://doi.org/10.1016/j.tws.2016.05.025.

Chen, D., Yang, J. and Kitipornchai, S. (2016), "Free and forced vibrations of shear deformable functionally graded porous beams", *Int. J. Mech. Sci.*, **108-109**, 14-22. https://doi.org/10.1016/j.ijmecsci.2016.01.025

Cong, P.H., Chien, T.M., Khoa, N.D. and Duc, N.D. (2018), "Nonlinear thermomechanical buckling and post-buckling response of porous FGM plates using Reddy's HSDT", *Aerosp. Sci. Technol.*, **77**, 419-428. https://doi.org/10.1016/j.ast.2018.03.020.

Detournay, E. and Cheng, A.H.D. (1995), "Fundamentals of poroelasticity", *Anal. Design Methods*, **1993**, 113-171. https://doi.org/10.1016/B978-0-08-040615-2.50011-3.

Do, T.V., Bui, T.Q., Yu, T.T., Pham, D.T. and Nguyen, C.T. (2017), "Role of material combination and new results of mechanical behavior for FG sandwich plates in thermal environment", *J. Comput. Sci.*, **21**, 164-181. https://doi.org/10.1016/j.jocs.2017.06.015.

Duc, N.D., Dinh Nguyen, P. and Dinh Khoa, N. (2017), "Nonlinear dynamic analysis and vibration of eccentrically stiffened S-FGM elliptical cylindrical shells surrounded on elastic foundations in thermal environments", *Thin Wall. Struct.*, **117**, 178-189. https://doi.org/10.1016/j.tws.2017.04.013.

Duc, N.D, Quang, V.D., Nguyen, P.D. and Chien, T.M. (2018), "Nonlinear dynamic response of functional graded porous plates on elastic foundation subjected to thermal and mechanical loads", *J. Appl. Comput. Mech.*, **4**(4), 245-259.

Duc, N.D. (2013), "Nonlinear dynamic response of imperfect eccentrically stiffened FGM double curved shallow shells on elastic foundation", *Compos. Struct.*, **99**, 88-96. https://doi.org/10.1016/j.compstruct.2012.11.017.

Duc, N.D. (2014), "Nonlinear static and dynamic stability of functionally graded plates and shells", *Vietnam National University Press.*

Duc, N.D. (2016), "Nonlinear thermal dynamic analysis of eccentrically stiffened S-FGM circular cylindrical shells surrounded on elastic foundations using the Reddy's third-order shear deformation shell theory", *Eur. J. Mech. - A - Solids*, **58**, 10-30. https://doi.org/10.1016/j.euromechsol.2016.01.004.

Duc, N.D. (2018), "Nonlinear thermo- electro-mechanical dynamic response of shear deformable piezoelectric sigmoid

functionally graded sandwich circular cylindrical shells on elastic foundations", *J. Sandw. Struct. Mater.*, **20**(3), 351-378. https://doi.org/10.1177/1099636216653266.

Duc, N.D. and Quan, T.Q. (2015), "Nonlinear dynamic analysis of imperfect FGM double curved thin shallow shells with temperature-dependent properties on elastic foundation", *J. Vib. Control*, **21**(7), 1340-1362.

Ebrahimi, F., Jafari, A. and Barati, M.R. (2017a), "Vibration analysis of magneto-electro-elastic heterogeneous porous material plates resting on elastic foundations", *Thin Wall. Struct.*, **119**, 33-46. https://doi.org/10.1016/j.tws.2017.04.002.

Ebrahimi, F., Daman, M. and Jafari, A. (2017b), "Nonlocal strain gradient-based vibration analysis of embedded curved porous piezoelectric nano-beams in thermal environment", *Smart Struct. Syst.*, **20**(6), 709-728. https://doi.org/10.12989/sss.2017.20.6.709.

Ellali, M., Amara, K., Bouazza, M. and Bourada, F. (2018), "The buckling of piezoelectric plates on pasternak elastic foundation using higher-order shear deformation plate theories", *Smart Struct. Syst.*, **21**(1), 113-122. https://doi.org/10.12989/sss.2018.21.1.113.

Eringen, A.C. (1983), "On differential equations of nonlocal elasticity and solutions of screw dislocation and surface waves", *J. Appl. Phys.*, **54**(9), 4703-4710. https://doi.org/10.1063/1.332803.

Eringen, A.C. (2002), *Nonlocal continuum field theories*. Springer Science & Business Media.

Ferreira, A.J.M., Fasshauer, G.E., Batra, R.C. and Rodrigues, J.D. (2008), "Static deformations and vibration analysis of composite and sandwich plates using a layerwise theory and RBF-PS discretizations with optimal shape parameter", *Compos. Struct.*, **86**(4), 328-343.

Ferreira, A.J.M., Viola, E., Tornabene, F., Fantuzzi, N. and Zenkour, A.M. (2013), "Analysis of sandwich plates by generalized differential quadrature method", *Math. Probl. Eng.*, **2013**, 1-12. http://dx.doi.org/10.1155/2013/964367.

Ghorbanpour-Arani, A. and Zamani, M.H. (2018), "Nonlocal free vibration analysis of FG-porous shear and normal deformable sandwich nanoplate with piezoelectric face sheets resting on silica aerogel foundation", *Arabian J. Sci. Eng.*, **43**(9), 4675-4688.

Ghorbanpour Arani, A., BabaAkbar Zarei, H. and Haghparast, E. (2018), "Vibration response of viscoelastic sandwich plate with magnetorheological fluid core and functionally graded-piezoelectric nanocomposite face sheets", *J. Vib. Control*, 107754631774750.

Ghorbanpour Arani, A., Roudbari, M.A. and Amir, S. (2016), "Longitudinal magnetic field effect on wave propagation of fluid-conveyed SWCNT using Knudsen number and surface considerations", *Appl. Math. Model.*, **40**(3), 2025-2038. https://doi.org/10.1016/j.apm.2015.09.055

Ghorbanpour Arani, A., Shajari, A., Amir, S. and Atabakhshian, V. (2013a), "Nonlinear fluid-induced vibration and instability of an embedded piezoelectric polymeric microtube using nonlocal elasticity theory", *Proceedings of the Institution of Mechanical Engineers, Part C: Journal of Mechanical Engineering Science*, **227**(12), 2870-2885.

Ghorbanpour Arani, A., Shirali, A., Farahani, M.N., Amir, S. and Loghman, A. (2013b), "Nonlinear vibration analysis of protein microtubules in cytosol conveying fluid based on nonlocal elasticity theory using differential quadrature method", *Proceedings of the Institution of Mechanical Engineers, Part C: Journal of Mechanical Engineering Science*, **227**(1), 137-145.

Ghorbanpour Arani, A. and Zamani, M.H. (2017), "Investigation of electric field effect on size-dependent bending analysis of functionally graded porous shear and normal deformable sandwich nanoplate on silica Aerogel foundation", *J. Sandw. Struct. Mater.*, 1099636217721405.

Iijima, S. (1991), "Helical microtubules of graphitic carbon", *Nature*, **354**(6348), 56.

Ke, L.L. and Wang, Y.S. (2014), "Free vibration of size-dependent magneto-electro-elastic nanobeams based on the nonlocal theory", *Physica E: Low-Dimens. Syst. Nanostruct.*, **63**, 52-61. https://doi.org/10.1016/j.physe.2014.05.002.

Ke, L.L., Wang, Y.S., Yang, J. and Kitipornchai, S. (2014), "Free vibration of size-dependent magneto-electro-elastic nanoplates based on the nonlocal theory", *Acta Mechanica Sinica*, **30**(4), 516-525.

Ke, L.L., Yang, J., Kitipornchai, S. and Bradford, M.A. (2012), "Bending, buckling and vibration of size-dependent functionally graded annular microplates", *Compos. Struct.*, **94**(11), 3250-3257. https://doi.org/10.1016/j.compstruct.2012.04.037.

Khorshidvand, A.R., Joubaneh, E.F., Jabbari, M. and Eslami, M.R. (2014), "Buckling analysis of a porous circular plate with piezoelectric sensor–actuator layers under uniform radial compression", *Acta Mechanica*, **225**(1), 179-193.

Kiran, M.C. and Kattimani, S.C. (2018), "Free vibration and static analysis of functionally graded skew magneto-electro-elastic plate", *Smart Struct. Syst.*, **21**(4), 493-519. https://doi.org/10.12989/sss.2018.21.4.493.

Kolahdouzan, F., Gorbanpour Arani, A. and Abdollahian, M. (2018), "Buckling and free vibration analysis of FG-CNTRC-micro sandwich plate", *Steel Compos. Struct.*, **26**(3), 273-287. https://doi.org/10.12989/scs.2018.26.3.273.

Lal, R. and Ahlawat, N. (2015), "Axisymmetric vibrations and buckling analysis of functionally graded circular plates via differential transform method", *Eur. J. Mech. – A- Solids*, **52**, 85-94. https://doi.org/10.1016/j.euromechsol.2015.02.004

Leclaire, P., Horoshenkov, K.V., Swift, M.J. and Hothersall, D.C. (2001), "The vibrational response of a clamped rectangular porous plate", *J. Sound Vib.*, **247**(1), 19-31. https://doi.org/10.1006/jsvi.2000.3657.

Lei, Z.X., Liew, K.M. and Yu, J.L. (2013), "Free vibration analysis of functionally graded carbon nanotube-reinforced composite plates using the element-free kp-Ritz method in thermal environment", *Compos. Struct.*, **106**, 128-138. https://doi.org/10.1016/j.compstruct.2013.06.003.

Leissa, A.W. (1969), *Vibration of plates*. Ohio State Univ. Columbus.

Liew, K.M., Han, J.B., Xiao, Z.M. and Du, H. (1996), "Differential quadrature method for Mindlin plates on Winkler foundations", *Int. J. Mech. Sci.*, **38**(4), 405-421. https://doi.org/10.1016/0020-7403(95)00062-3.

Liu, S., Yu, T., Bui, T.Q. and Xia, S. (2017a), "Size-dependent analysis of homogeneous and functionally graded microplates using IGA and a non-classical Kirchhoff plate theory", *Compos. Struct.*, **172**, 34-44. https://doi.org/10.1016/j.compstruct.2017.03.067.

Liu, S., Yu, T. and Bui, T.Q. (2017b), "Size effects of functionally graded moderately thick microplates: A novel non-classical simple-FSDT isogeometric analysis", *Eur. J. Mech. – A - Solids*, **66**, 446-458. https://doi.org/10.1016/j.euromechsol.2017.08.008.

Liu, S., Yu, T., Lich, L. Van, Yin, S. and Bui, T.Q. (2019), "Size and surface effects on mechanical behavior of thin nanoplates incorporating microstructures using isogeometric analysis", *Comput. Struct.*, **212**, 173-187. https://doi.org/10.1016/j.compstruc.2018.10.009.

Liu, S., Yu, T., Van Lich, L., Yin, S. and Bui, T.Q. (2018), "Size effect on cracked functional composite micro-plates by an XIGA-based effective approach", *Meccanica*, **53**(10), 2637-2658.

Loghman, A. and Cheraghbak, A. (2018), "Agglomeration effects on electro-magneto-thermo elastic behavior of nano-composite piezoelectric cylinder", *Polymer Compos.*, **39**(5), 1594-1603.

https://doi.org/10.1002/pc.24104.

Loghman, A., Ghorbanpour Arani, A. and Mosallaie Barzoki, A. (2017), "Nonlinear stability of non-axisymmetric functionally graded reinforced nano composite microplates", *Comput. Concrete*, **19**(6), 677-687. https://doi.org/10.12989/cac.2017.19.6.677.

Malekzadeh, P. and Zarei, A.R. (2014), "Free vibration of quadrilateral laminated plates with carbon nanotube reinforced composite layers", *Thin Wall. Struct.*, **82**, 221-232. https://doi.org/10.1016/j.tws.2014.04.016.

Mechab, I., Mechab, B., Benaissa, S., Serier, B. andBouiadjra, B. B. (2016), "Free vibration analysis of FGM nanoplate with porosities resting on Winkler Pasternak elastic foundations based on two-variable refined plate theories", *J. Braz. Soc. Mech. Sci. Eng.*, **38**(8), 2193-2211.

Mehar, K., Panda, S.K., Bui, T.Q. and Mahapatra, T.R. (2017), "Nonlinear thermoelastic frequency analysis of functionally graded CNT-reinforced single/doubly curved shallow shell panels by FEM", *J. Therm. Stresses*, **40**(7), 899-916. https://doi.org/10.1080/01495739.2017.1318689.

Meirovitch, L. (1997), *Principles and techniques of vibrations* (Vol. 1). Prentice Hall New Jersey.

Mirzaei, M. and Kiani, Y. (2016), "Free vibration of functionally graded carbon nanotube reinforced composite cylindrical panels", *Compos. Struct.*, **142**, 45-56. https://doi.org/10.1016/j.compstruct.2015.12.071.

Mohammadzadeh-Keleshteri, M., Asadi, H. and Aghdam, M.M. (2017), "Geometrical nonlinear free vibration responses of FG-CNT reinforced composite annular sector plates integrated with piezoelectric layers", *Compos. Struct.*, **171**, 100-112. https://doi.org/10.1016/j.compstruct.2017.01.048.

Pham, T. Van and Duc, N.D. (2016), "Nonlinear stability analysis of imperfect three-phase sandwich laminated polymer nanocomposite panels resting on elastic foundations in thermal environments", *VNU J. Sci.: Math. Phys.*, **32**(1), 20-36.

Quan, T.Q., Tran, P., Tuan, N.D. and Duc, N.D. (2015), "Nonlinear dynamic analysis and vibration of shear deformable eccentrically stiffened S-FGM cylindrical panels with metal-ceramic-metal layers resting on elastic foundations", *Compos. Struct.*, **126**, 16-33. https://doi.org/10.1016/j.compstruct.2015.02.056.

Reddy, J.N. and Berry, J. (2012), "Nonlinear theories of axisymmetric bending of functionally graded circular plates with modified couple stress", *Compos. Struct.*, **94**(12), 3664-3668. https://doi.org/10.1016/j.compstruct.2012.04.019.

Reddy, J.N. and Khdeir, A. (1989), "Buckling and vibration of laminated composite plates using various plate theories", *AIAA J.*, **27**(12), 1808-1817. https://doi.org/10.2514/3.10338.

Reddy, J., Wang, C. and Kitipornchai, S. (1999), "Axisymmetric bending of functionally graded circular and annular plates", *Eur. J. Mech. –A - Solids*, **18**(2), 185-199. https://doi.org/10.1016/S0997-7538(99)80011-4.

Rezaei, A.S. and Saidi, A.R. (2015), "Exact solution for free vibration of thick rectangular plates made of porous materials", *Compos.Struct.*, **134**, 1051-1060. https://doi.org/10.1016/j.compstruct.2015.08.125.

Shafiei, N. and Kazemi, M. (2017), "Buckling analysis on the bi-dimensional functionally graded porous tapered nano-/micro-scale beams", *Aerosp. Sci. Technol.*, **66**, 1-11. https://doi.org/10.1016/j.ast.2017.02.019.

Shafiei, N., Mirjavadi, S.S., MohaselAfshari, B., Rabby, S. and Kazemi, M. (2017), "Vibration of two-dimensional imperfect functionally graded (2D-FG) porous nano-/micro-beams", *Comput. Method. Appl. M.*, **322**, 615-632. https://doi.org/10.1016/j.cma.2017.05.007.

Shahverdi, H. and Barati, M.R. (2017), "Vibration analysis of porous functionally graded nanoplates", *Int. J. Eng. Science*, **120**, 82-99. https://doi.org/10.1016/j.ijengsci.2017.06.008.

Sidhoum, I.A., Boutchicha, D., Benyoucef, S. and Tounsi, A. (2018), "A novel quasi-3D hyperbolic shear deformation theory for vibration analysis of simply supported functionally graded plates", *Smart Struc. Syst.*, **22**(3), 303-314. https://doi.org/10.12989/gae.2017.12.1.009

Shu, C. (2012), *Differential quadrature and its application in engineering*. Springer Science & Business Media.

Theodorakopoulos, D.D. and Beskos, D.E. (1994), "Flexural vibrations of poroelastic plates", *Acta Mechanica*, **103**(1-4), 191-203.

Tohidi, H., Hosseini-Hashemi, S.H. and Maghsoudpour, A. (2018), "Size-dependent forced vibration response of embedded micro cylindrical shells reinforced with agglomerated CNTs using strain gradient theory", *Smart Struct. Syst.*, **22**(5), 527-546. https://doi.org/10.12989/sss.2018.22.5.527.

Wang, Z.X. and Shen, H.S. (2012), "Nonlinear vibration and bending of sandwich plates with nanotube-reinforced composite face sheets", *Compos. Part B: Eng.*, **43**(2), 411-421. https://doi.org/10.1016/j.compositesb.2011.04.040.

Wu, T., Wang, Y. and Liu, G. (2002), "Free vibration analysis of circular plates using generalized differential quadrature rule", *Comput. Method. Appl. M.*, **191**(46), 5365-5380. https://doi.org/10.1016/S0045-7825(02)00463-2.

Yazid, M., Heireche, H., Tounsi, A., Bousahla, A.A. andHouari, M. S.A. (2018), "A novel nonlocal refined plate theory for stability response of orthotropic single-layer graphene sheet resting on elastic medium", *Smart Struct. Syst.*, **21**(1), 15-25. https://doi.org/10.12989/sss.2018.21.1.015.

Yu, T., Hu, H., Zhang, J. and Bui, T.Q. (2019a), "Isogeometric analysis of size-dependent effects for functionally graded microbeams by a non-classical quasi-3D theory", *Thin Wall. Struct.*, **138**, 1-14. https://doi.org/10.1016/j.tws.2018.12.006

Yu, T., Zhang, J., Hu, H. and Bui, T.Q. (2019b), "A novel size-dependent quasi-3D isogeometric beam model for two-directional FG microbeams analysis", *Compos. Struct.*, **211**, 76-88. https://doi.org/10.1016/j.compstruct.2018.12.014.

Zhou, D., Au, F.T.K., Cheung, Y.K. and Lo, S.H. (2003), "Three-dimensional vibration analysis of circular and annular plates via the Chebyshev–Ritz method", *Int. J. Solids Struct.*, **40**(12), 3089-3105. https://doi.org/10.1016/S0020-7683(03)00114-8.

Zhou, Z.H., Wong, K.W., Xu, X.S. and Leung, A.Y.T. (2011), "Natural vibration of circular and annular thin plates by Hamiltonian approach", *J. Sound Vib.*, **330**(5), 1005-1017. https://doi.org/10.1016/j.jsv.2010.09.015.

Zhu, P., Lei, Z.X. and Liew, K.M. (2012), "Static and free vibration analyses of carbon nanotube-reinforced composite plates using finite element method with first order shear deformation plate theory", *Compos. Struct.*, **94**(4), 1450-1460. https://doi.org/10.1016/j.compstruct.2011.11.010.

CC

Funding

The authors are thankful to the University of Kashan for supporting this work by Grant No. 891255/1.

Appendix

The used coefficients in Eqs. (65)-(69) are defined as follow

$$P_1=\int_{-\frac{h_c}{2}-h_b}^{-\frac{h_c}{2}} Q_{11}^{b}\,\mathrm{d}z+\int_{-\frac{h_c}{2}}^{\frac{h_c}{2}} A_1(z)\,\mathrm{d}z+\int_{\frac{h_c}{2}}^{\frac{h_c}{2}+h_t} Q_{11}^{t}\,\mathrm{d}z,$$

$$P_2=\int_{-\frac{h_c}{2}-h_b}^{-\frac{h_c}{2}} Q_{22}^{b}\,\mathrm{d}z+\int_{-\frac{h_c}{2}}^{\frac{h_c}{2}} A_1(z)\,\mathrm{d}z+\int_{\frac{h_c}{2}}^{\frac{h_c}{2}+h_t} Q_{22}^{t}\,\mathrm{d}z,$$

$$P_3=\int_{-\frac{h_c}{2}-h_b}^{-\frac{h_c}{2}} Q_{11}^{b}\,z\,\mathrm{d}z+\int_{-\frac{h_c}{2}}^{\frac{h_c}{2}} A_1(z)\,z\,\mathrm{d}z+\int_{\frac{h_c}{2}}^{\frac{h_c}{2}+h_t} Q_{11}^{t}\,z\,\mathrm{d}z,$$

$$P_4=\int_{-\frac{h_c}{2}-h_b}^{-\frac{h_c}{2}} Q_{22}^{b}\,z\,\mathrm{d}z+\int_{-\frac{h_c}{2}}^{\frac{h_c}{2}} A_1(z)\,z\,\mathrm{d}z+\int_{\frac{h_c}{2}}^{\frac{h_c}{2}+h_t} Q_{22}^{t}\,z\,\mathrm{d}z,$$

$$P_5=\int_{-\frac{h_c}{2}-h_b}^{-\frac{h_c}{2}} Q_{55}^{b}\,\mathrm{d}z+\int_{-\frac{h_c}{2}}^{\frac{h_c}{2}} G(z)\,\mathrm{d}z+\int_{\frac{h_c}{2}}^{\frac{h_c}{2}+h_t} Q_{55}^{t}\,\mathrm{d}z,$$

$$P_6=\int_{-\frac{h_c}{2}-h_b}^{-\frac{h_c}{2}} Q_{11}^{b}\,z^2\,\mathrm{d}z+\int_{-\frac{h_c}{2}}^{\frac{h_c}{2}} A_1(z)\,z^2\,\mathrm{d}z+\int_{\frac{h_c}{2}}^{\frac{h_c}{2}+h_t} Q_{11}^{t}\,z^2\,\mathrm{d}z,$$

$$P_7=\int_{-\frac{h_c}{2}-h_b}^{-\frac{h_c}{2}} Q_{22}^{b}\,z^2\,\mathrm{d}z+\int_{-\frac{h_c}{2}}^{\frac{h_c}{2}} A_1(z)\,z^2\,\mathrm{d}z+\int_{\frac{h_c}{2}}^{\frac{h_c}{2}+h_t} Q_{22}^{t}\,z^2\,\mathrm{d}z,$$

$$E_1=\int_{-\frac{h_c}{2}-h_b}^{-\frac{h_c}{2}} e_{31}^{b}\left[\frac{\pi}{h_b}\right]\sin\left(\frac{\pi z_b}{h_b}\right)\mathrm{d}z+\int_{\frac{h_c}{2}}^{\frac{h_c}{2}+h_t} e_{31}^{t}\left[\frac{\pi}{h_t}\right]\sin\left(\frac{\pi z_t}{h_t}\right)\mathrm{d}z,$$

$$E_2=\int_{-\frac{h_c}{2}-h_b}^{-\frac{h_c}{2}} e_{32}^{b}\left[\frac{\pi}{h_b}\right]\sin\left(\frac{\pi z_b}{h_b}\right)\mathrm{d}z+\int_{\frac{h_c}{2}}^{\frac{h_c}{2}+h_t} e_{32}^{t}\left[\frac{\pi}{h_t}\right]\sin\left(\frac{\pi z_t}{h_t}\right)\mathrm{d}z,$$

$$E_3=\int_{-\frac{h_c}{2}-h_b}^{-\frac{h_c}{2}} e_{15}^{b}\cos\left(\frac{\pi z_b}{h_b}\right)\mathrm{d}z+\int_{\frac{h_c}{2}}^{\frac{h_c}{2}+h_t} e_{15}^{t}\cos\left(\frac{\pi z_t}{h_t}\right)\mathrm{d}z,$$

$$E_4=\int_{-\frac{h_c}{2}-h_b}^{-\frac{h_c}{2}} e_{31}^{b}\left[\frac{\pi}{h_b}\right]\sin\left(\frac{\pi z_b}{h_b}\right)z\,\mathrm{d}z+\int_{\frac{h_c}{2}}^{\frac{h_c}{2}+h_t} e_{31}^{t}\left[\frac{\pi}{h_t}\right]\sin\left(\frac{\pi z_t}{h_t}\right)z\,\mathrm{d}z,$$

$$E_5=\int_{-\frac{h_c}{2}-h_b}^{-\frac{h_c}{2}} e_{32}^{b}\left[\frac{\pi}{h_b}\right]\sin\left(\frac{\pi z_b}{h_b}\right)z\,\mathrm{d}z+\int_{\frac{h_c}{2}}^{\frac{h_c}{2}+h_t} e_{32}^{t}\left[\frac{\pi}{h_t}\right]\sin\left(\frac{\pi z_t}{h_t}\right)z\,\mathrm{d}z,$$

$$E_6=\int_{-\frac{h_c}{2}-h_b}^{-\frac{h_c}{2}} s_{11}^{b}\cos^2\left(\frac{\pi z_b}{h_b}\right)\mathrm{d}z+\int_{\frac{h_c}{2}}^{\frac{h_c}{2}+h_t} s_{11}^{t}\cos^2\left(\frac{\pi z_t}{h_t}\right)\mathrm{d}z,$$

$$E_7=\int_{-\frac{h_c}{2}-h_b}^{-\frac{h_c}{2}} s_{33}^{b}\left[\frac{\pi}{h_b}\right]^2\sin^2\left(\frac{\pi z_b}{h_b}\right)z\,\mathrm{d}z+\int_{\frac{h_c}{2}}^{\frac{h_c}{2}+h_t} s_{33}^{t}\left[\frac{\pi}{h_t}\right]^2\sin^2\left(\frac{\pi z_t}{h_t}\right)z\,\mathrm{d}z,$$

$$H_1=\int_{-\frac{h_c}{2}-h_b}^{-\frac{h_c}{2}} q_{31}^{b}\left[\frac{\pi}{h_b}\right]\sin\left(\frac{\pi z_b}{h_b}\right)\mathrm{d}z+\int_{\frac{h_c}{2}}^{\frac{h_c}{2}+h_t} q_{31}^{t}\left[\frac{\pi}{h_t}\right]\sin\left(\frac{\pi z_t}{h_t}\right)\mathrm{d}z,$$

$$H_2=\int_{-\frac{h_c}{2}-h_b}^{-\frac{h_c}{2}} q_{32}^{b}\left[\frac{\pi}{h_b}\right]\sin\left(\frac{\pi z_b}{h_b}\right)\mathrm{d}z+\int_{\frac{h_c}{2}}^{\frac{h_c}{2}+h_t} q_{32}^{t}\left[\frac{\pi}{h_t}\right]\sin\left(\frac{\pi z_t}{h_t}\right)\mathrm{d}z,$$

$$H_3=\int_{-\frac{h_c}{2}-h_b}^{-\frac{h_c}{2}} q_{15}^{b}\cos\left(\frac{\pi z_b}{h_b}\right)\mathrm{d}z+\int_{\frac{h_c}{2}}^{\frac{h_c}{2}+h_t} q_{15}^{t}\cos\left(\frac{\pi z_t}{h_t}\right)\mathrm{d}z,$$

$$H_4=\int_{-\frac{h_c}{2}-h_b}^{-\frac{h_c}{2}} q_{31}^{b}\left[\frac{\pi}{h_b}\right]\sin\left(\frac{\pi z_b}{h_b}\right)z\,\mathrm{d}z+\int_{\frac{h_c}{2}}^{\frac{h_c}{2}+h_t} q_{31}^{t}\left[\frac{\pi}{h_t}\right]\sin\left(\frac{\pi z_t}{h_t}\right)z\,\mathrm{d}z,$$

$$H_5=\int_{-\frac{h_c}{2}-h_b}^{-\frac{h_c}{2}} q_{32}^{b}\left[\frac{\pi}{h_b}\right]\sin\left(\frac{\pi z_b}{h_b}\right)z\,\mathrm{d}z+\int_{\frac{h_c}{2}}^{\frac{h_c}{2}+h_t} q_{32}^{t}\left[\frac{\pi}{h_t}\right]\sin\left(\frac{\pi z_t}{h_t}\right)z\,\mathrm{d}z,$$

$$H_6=\int_{-\frac{h_c}{2}-h_b}^{-\frac{h_c}{2}} d_{11}^{b}\cos^2\left(\frac{\pi z_b}{h_b}\right)\mathrm{d}z+\int_{\frac{h_c}{2}}^{\frac{h_c}{2}+h_t} d_{11}^{t}\cos^2\left(\frac{\pi z_t}{h_t}\right)\mathrm{d}z,$$

$$H_7=\int_{-\frac{h_c}{2}-h_b}^{-\frac{h_c}{2}} d_{33}^{b}\left[\frac{\pi}{h_b}\right]^2\sin^2\left(\frac{\pi z_b}{h_b}\right)z\,\mathrm{d}z+\int_{\frac{h_c}{2}}^{\frac{h_c}{2}+h_t} d_{33}^{t}\left[\frac{\pi}{h_t}\right]^2\sin^2\left(\frac{\pi z_t}{h_t}\right)z\,\mathrm{d}z,$$

$$R_1=\int_{-\frac{h_c}{2}-h_b}^{-\frac{h_c}{2}} \mu_{11}^{b}\cos^2\left(\frac{\pi z_b}{h_b}\right)\mathrm{d}z+\int_{\frac{h_c}{2}}^{\frac{h_c}{2}+h_t} \mu_{11}^{t}\cos^2\left(\frac{\pi z_t}{h_t}\right)\mathrm{d}z,$$

$$R_2=\int_{-\frac{h_c}{2}-h_b}^{-\frac{h_c}{2}} \mu_{33}^{b}\left[\frac{\pi}{h_b}\right]^2\cos^2\left(\frac{\pi z_b}{h_b}\right)\mathrm{d}z+\int_{\frac{h_c}{2}}^{\frac{h_c}{2}+h_t} \mu_{33}^{t}\left[\frac{\pi}{h_t}\right]^2\cos^2\left(\frac{\pi z_t}{h_t}\right)\mathrm{d}z$$